Research Square

Preprints are preliminary reports that have not undergone peer review.
They should not be considered conclusive, used to inform clinical practice,
or referenced by the media as validated information.

Hyaluronic Acid-Functionalized Cellulose Nanofiber-Stabilized Pickering Emulsion Incorporated into Sodium Alginate Coatings for Blueberry Preservation

Rahmah Muthiah Abdul Kholiq
Kyushu University
Francis Ngwane Nkede
Kyushu University
Mohammad Hamayoon Wardak
Kyushu University
Amna Bibi
Kyushu University
Ata Aditya Wardana
Binus University
Fanze Meng
Kyushu University
Fumina Tanaka
Kyushu University
Fumihiko Tanaka
fumit@bpes.kyushu-u.ac.jp

Kyushu University

Research Article

Keywords: Edible coatings, Hyaluronic acid-functionalized cellulose nanofibers, Pickering emulsions, Sodium alginate, Parsley essential oil, Postharvest blueberry preservation

Posted Date: November 4th, 2026

DOI: https://doi.org/10.21203/rs.3.rs-11430481/v1

License: This work is licensed under a Creative Commons Attribution 4.0 International License.
Read Full License

Additional Declarations: No competing interests reported.

Hyaluronic Acid-Functionalized Cellulose Nanofiber-Stabilized Pickering Emulsion Incorporated into Sodium Alginate Coatings for Blueberry Preservation

Rahmah Muthiah Abdul Kholiq[a], Francis Ngwane Nkede[b*], Mohammad Hamayoon Wardak[b], Amna Bibi[a], Ata Aditya Wardana[c], Fanze Meng[b], Fumina Tanaka[b], and Fumihiko Tanaka[b*]

[a] Graduate School of Bioresource and Bioenvironmental Sciences, Kyushu University, 744, Motooka, Nishi-ku, Fukuoka-shi, Fukuoka, 819-0395, Japan

[b] Laboratory of Postharvest Science, Faculty of Agriculture, Kyushu University, 744, Motooka, Nishi-ku, Fukuoka-shi, Fukuoka 819–0395, Japan

[c] Department of Food Technology, Faculty of Engineering, Bina Nusantara University, Jakarta, 11480, Indonesia

[*] Corresponding authors.

E-mail addresses: fumit@bpes.kyushu-u.ac.jp (Fumihiko Tanaka)

nkedefrancis1@gmail.com (Francis Ngwane Nkede)

Abstract

The development of sustainable postharvest technologies is essential for reducing food losses while minimizing reliance on synthetic packaging materials. In this study, a hyaluronic acid (HA)-functionalized, cellulose nanofiber (CNF)-stabilized Pickering emulsion edible coating was formulated using sodium alginate as the film-forming matrix and parsley essential oil as the bioactive component. Ultrasound was employed as an emulsification aid during preparation, and the resulting formulations exhibited strong electrostatic stability, with zeta-potential values ranging from −40.13 to −82.87 mV, together with favorable oil-binding

capacity. HA functionalization promoted uniform droplet dispersion and contributed to the formation of a compact polymer network. Among the formulations, SA/0.5 HA-PE showed the highest oil-binding capacity, the lowest water vapor permeability, and the most homogeneous internal structure. When applied to blueberries stored at 25 °C for 10 days, the coating reduced weight loss to 8.07–8.42% compared with 13.30% in the control, while also contributing to firmness retention, physicochemical quality preservation, and inhibition of fungal deterioration. Correlation and principal component analyses indicated associations among moisture loss, firmness, and other quality attributes during storage. Overall, the results demonstrate the potential of the ultrasound-assisted HA-functionalized CNF Pickering emulsion coating as a bio-based approach for blueberry preservation. However, because a non-ultrasound control was not included, the specific contribution of ultrasound to the observed emulsion and coating properties cannot be isolated.

Keywords: Edible coatings; Hyaluronic acid-functionalized cellulose nanofibers; Pickering emulsions; Sodium alginate; Parsley essential oil; Postharvest blueberry preservation

Introduction

Fresh fruits are nutrient-dense, with recommended daily intakes of 100–300 g, however, their high perishability contributes substantially to global food loss, resource inefficiency, and environmental burdens. Fruits and vegetables account for nearly one-third of global food waste (Porat et al. 2018; Santos et al. 2020), driven by physiological activity, moisture depletion, microbial contamination, and oxidative stress (Ali et al. 2025). These losses reduce

food availability and economic value, underscoring the need for sustainable preservation strategies that maintain fruit quality while reducing reliance on synthetic packaging.

Blueberries (*Vaccinium* spp.) are high-value fruits rich in anthocyanins, phenolic acids, flavonoids, vitamins, and dietary fiber, which contribute to their antioxidant and health-promoting properties (Ashique et al. 2024; Stull et al. 2024). Despite increasing global production, their delicate epidermis, high respiration rate, elevated moisture content and non-climacteric nature make them highly susceptible to postharvest deterioration (Ding et al. 2024a; Li et al. 2021). Mechanical injury, dehydration, softening, microbial spoilage, and oxidative degradation further reduce marketability, particularly under ambient storage. Conventional preservation methods—including refrigeration, modified-atmosphere packaging, synthetic fungicides, and plastic-based packaging—remain effective but raise concerns regarding environmental persistence, energy intensity, and human exposure (Cao et al. 2025; Jiang et al. 2023; Li et al. 2025). Growing consumer demand for minimally processed and sustainably packaged foods has accelerated interest in biodegradable, renewable, and edible preservation systems.

Edible coatings offer a promising alternative because they are biodegradable (Kusuma et al. 2024) and capable of regulating gas exchange (Phuong et al. 2023), reducing moisture loss (Bibi et al. 2026), and inhibiting oxidation (Takahashi et al. 2024) and microbial deterioration (Wardak et al. 2024). Their ability to deliver natural bioactives further enhances preservation efficacy. However, many polysaccharide-based coatings exhibit limited mechanical strength, modest water-vapor barriers, and poor stability of hydrophobic actives, highlighting the need for next-generation coating technologies.

Sodium alginate (SA) is widely used in edible coatings due to its biodegradability, non-toxicity, film-forming ability, and compatibility with diverse bioactive compounds (Das et al. 2020; Nkede et al. 2023; Panahi and Mohsenzadeh 2022; Wardak et al. 2024). Despite its good oxygen-barrier properties, SA is highly hydrophilic and exhibits limited moisture resistance and mechanical robustness, motivating incorporation of functional polymers and nanomaterials to reinforce its matrix.

Cellulose nanofibers (CNFs) are renewable nanomaterials with high aspect ratio, mechanical strength, biodegradability, and abundant surface hydroxyl groups (Wang et al. 2024). Beyond strengthening polymer matrices, CNFs act as efficient solid-particle stabilizers for Pickering emulsions (PEs), which rely on irreversible particle adsorption at the oil–water interface rather than synthetic surfactants (Nkede, et al. 2023a; Wen et al. 2023; Wigati et al. 2023; Wu et al. 2024). Pickering emulsions enhance resistance to coalescence and provide an effective platform for encapsulating hydrophobic bioactive compounds, improving their dispersibility, stability, and functionality.

Parsley essential oil (PEO) contains phenylpropanoids and terpenoids with well-established antimicrobial and antioxidant activities (Kobasy et al. 2025; Semeniuc et al. 2017; Wong and Kitts 2006a). However, its practical use is limited by poor solubility, volatility, and oxidation susceptibility—constraints that can be mitigated through encapsulation within Pickering emulsions.

Hyaluronic acid (HA), a biocompatible polysaccharide with strong water-binding capacity, can strengthen interfacial layers, improve steric stabilization, and promote uniform coating microstructures (Cao et al. 2026; Wang et al. 2023). Although HA has demonstrated

functional benefits in hydrogel and polysaccharide systems, its role within CNF-stabilized Pickering emulsions for edible coatings remains unexplored.

Ultrasound processing can facilitate emulsification through cavitation-induced shear and improved dispersion of the dispersed phase (Cheng et al. 2024; Liu et al. 2025). However, the magnitude of its contribution depends on processing conditions and requires appropriate non-ultrasound controls for direct attribution. In the present study, ultrasound was employed as an emulsification aid during preparation of the HA-functionalized CNF Pickering emulsion. Therefore, the observed properties should be interpreted as the performance of the ultrasound-assisted formulation rather than as evidence of an independent ultrasound effect.

To the best of our knowledge, this is the first study to investigate a hyaluronic acid-functionalized, cellulose nanofiber-stabilized Pickering emulsion incorporated into an edible coating for blueberry preservation using ultrasound-assisted emulsification. The study therefore focuses on the resulting emulsion, film, and postharvest performance, while recognizing that the specific contribution of ultrasound cannot be isolated in the absence of a non-ultrasound control. This gap is particularly critical for highly perishable and non-climacteric fruits such as blueberries, where rapid moisture loss and microbial decay accelerate waste (Ding et al. 2024a; Li et al. 2021).

Based on this gap, we developed a HA-functionalized CNF Pickering-emulsion edible coating using sodium alginate as the film-forming matrix and parsley essential oil as the encapsulated bioactive compound, with ultrasound used as an emulsification aid. Emulsion characteristics and stability were first examined, followed by evaluation of the coating's effectiveness in preserving blueberry quality under ambient storage conditions. We

hypothesized that HA functionalization would improve interfacial stabilization and oil retention within the CNF-stabilized Pickering emulsion, thereby contributing to improved coating barrier properties and blueberry shelf-life performance. Because a non-ultrasound control was not included, the independent contribution of ultrasound was not hypothesized or quantified.

2. Materials and Methods

2.1. Materials

Sodium alginate (SA) was obtained from Fujifilm Chemical Industries Ltd. (Tokyo, Japan). Food-grade glycerol was purchased from Wako Pure Chemical Industries, Ltd. (Osaka, Japan). Hyaluronic acid (HA) was sourced from Nichiei Co., Ltd. (Nagoya, Japan), and cellulose nanofibers (CNFs) were supplied by Nippon Paper Industries Co., Ltd. (Japan). Parsley essential oil (PEO; 100% purity) was acquired from a certified commercial supplier. Potato dextrose agar (PDA) was obtained from Shimadzu Diagnostics Corporation (Tokyo, Japan) and used as the culture medium for fungal assays. *Botrytis cinerea* (NBRC 100717) was provided by the Biological Resource Center of the National Institute of Technology and Evaluation (Tokyo, Japan). Fresh blueberries of uniform size, color, and maturity, free from visible defects, were sourced from a local farmer in Fukuoka, Japan, transported to the laboratory, and used immediately to ensure consistency in postharvest quality assessments.

2.2. Preparation of HA-functionalized CNF-stabilized PEs

An aqueous CNF dispersion (0.24%, w/v) was prepared by dispersing CNF powder in distilled water under magnetic stirring (1500 rpm, 20 min) at room temperature, followed by ultrasonication (40 kHz, 20 min) to ensure complete fibril separation. HA was added to the

CNF dispersion at 0.2% or 0.5% (w/v) and stirred for 50 min to allow full hydration and promote HA–CNF interactions, yielding HA-functionalized CNF suspensions. Parsley essential oil (PEO; 0.1%, v/v) was then incorporated and pre-homogenized (10,000 rpm, 3 min) to form a coarse emulsion. Final emulsification was achieved by ultrasonic treatment using a 2510J–MTH unit (40 kHz, 100 W, 20 min). An ice bath was used throughout processing to maintain temperatures below 30 °C and prevent thermal degradation of the biopolymer matrix.

2.3. Preparation of coating solution and film

A sodium alginate solution (1.25%, w/v) was prepared following a modified version of our previous protocol (Nkede et al., 2023). SA was dissolved in distilled water under continuous stirring at 60 °C (430 rpm) using a Heidon Agitator (BL600, Japan) until fully solubilized. Glycerol (0.35%, v/v) was added as a plasticizer and mixed for an additional 20 min. The prepared Pickering emulsions (PEs) were then gradually incorporated into the SA solution under stirring (1500 rpm, 15–20 min) to ensure homogeneous dispersion. Entrapped air was removed using a vacuum chamber (Yamato ADP 300, Japan) to improve coating uniformity. For film formation, 25 mL of each coating solution was cast onto leveled polystyrene Petri dishes (90 mm diameter) and dried at 30 °C for 17 h. The dried films were peeled carefully and conditioned in a desiccator containing saturated potassium nitrate for 48 h to equilibrate moisture content prior to characterization. The final formulations consisting of SA/0.2 HA, SA/0.5 HA, SA/0.2 HA-PE, and SA/0.5 HA-PE—reflected variations in HA concentration and the presence or absence of Pickering emulsions.

2.4. Characterization of coating and film

2.4.1. Emulsion stability

Emulsion stability was assessed by transferring each coating formulation into 20 mL glass vials, sealing them, and storing them at room temperature for 8 days. Photographs were taken periodically to monitor phase separation, creaming, or sedimentation, providing a visual evaluation of physical stability within the film-forming system.

2.4.2. Zeta potential

Zeta potential was measured using a Zetasizer Nano ZS3600 (Malvern Instruments Inc., UK) to evaluate electrostatic interactions and colloidal stability. Measurements were performed in triplicate at room temperature following (Bibi et al. 2026).

2.4.3. Oil binding capacity (OBC)

OBC was determined using a modified method from (Cao et al. 2026). Film samples (~0.2 g) were weighed (W_0), immersed in 10 mL olive oil, and incubated at 25 °C for 24 h. Samples were centrifuged (3000 rpm, 20 min), blotted to remove surface oil, and reweighed (W_1). OBC was calculated using Eq. (1):

$$\text{OBC (g/g)} = \frac{W1 - W0}{W0} \quad (1)$$

where W_0 is the initial dry film weight and W_1 is the weight after oil binding.

2.4.4. Confocal Laser Scanning Microscopy (CLSM)

The spatial distribution of PEO within the film matrix was examined using confocal laser scanning microscopy (CLSM) following Wardak et al. (2025). Film samples (1 × 1 cm) were stained with Nile Red, mounted on microscope slides, and imaged using a Leica TCS SP8 system (Solms, Germany) equipped with a white-light laser and a 100× objective.

Fluorescence was recorded at 561 nm excitation and 550–600 nm emission, enabling visualization of hydrophobic domains and the distribution of PEO within the film microstructure.

2.4.5. Antifungal assay

Antifungal activity against *Botrytis cinerea* was evaluated using an in vitro assay adapted from Nkede et al. (2024). Potato dextrose agar (PDA) was prepared, autoclaved, and poured into sterile Petri dishes (20 mL per plate). *B. cinerea* was pre-cultured on PDA at 25 °C for 4 days to obtain actively growing mycelia. For testing, 10 mL molten PDA was mixed with 10 mL of each coating formulation, vortexed at 3000 rpm for 30 s, poured into sterile plates, and allowed to solidify. A 5 mm mycelial plug from the active culture was placed at the center of each plate. PDA mixed with sterile distilled water served as the negative control. Plates were incubated at 25 °C for 4 days, and mycelial growth was quantified by measuring colony diameter using ImageJ in triplicate.

2.4.6. Film Thickness

Film thickness was measured using a digital micrometer (Mitutoyo, Japan). Five random points were selected per film, and the mean value was recorded. Measurements were performed in quadruplicate following the protocol of Meng et al. (2024)

2.4.7. Color

Film color was evaluated using a CR-400 colorimeter (Konica Minolta, Japan). Measurements were taken at five random positions in quadruplicate and expressed in CIELAB coordinates (L*, a*, b*). Total color difference (ΔE) was calculated according to Eq. (2), following the protocol of Nkede et al. (2024).

$$\Delta E = [(L_{calibrated} - L_{sample})^2 + (a_{calibrated} - a_{sample})^2 + (b_{calibrated} - b_{sample})^2]^{1/2} \quad (2)$$

2.4.8. Scanning Electron Microscopy (SEM)

Surface and cross-sectional microstructures were examined using a scanning electron microscope (SU3500, Hitachi, Japan) following the method of Wardak et al. (2025). Film samples were mounted on aluminum stubs and sputter-coated with a thin conductive layer using an HPC-1SW osmium coater (Vacuum Device, Ibaraki, Japan). Micrographs were captured at an accelerating voltage of 12 kV to visualize structural features, interfacial organization, and coating uniformity.

2.4.9. Fourier transform infrared spectroscopy (FTIR)

FTIR spectra were recorded using an FT/IR-4700 spectrometer (Jasco, Japan) equipped with an ATR accessory. Spectra were collected over 4000–500 cm^{-1} following the protocol of Bibi et al. (2026). This analysis was used to identify functional groups and evaluate potential interactions among film components, providing insight into structural modifications within the biopolymer matrix.

2.4.10. Light barrier and opacity

Light transmittance was evaluated using a UV–Vis spectrophotometer (V730, Jasco, Tokyo, Japan) across 200–800 nm. Film samples were placed directly on the cuvette surface, and measurements were performed in triplicate. Opacity was calculated using absorbance at 600 nm and film thickness (Mitutoyo micrometer), following the method of Wardana et al. (2024). This analysis quantified the films' ability to block or attenuate light, an important functional attribute for active packaging materials.

$$\text{Opacity} = \frac{\text{A600}}{\text{Film thickness (mm)}} \quad (3)$$

2.4.11. Mechanical properties

Tensile strength (TS) and elongation at break (EAB) were measured using a universal testing machine (FGS-50EL, Nidec Shimpo Co., Japan). Film strips (5 × 1 cm²) were tested in seven replicates following the procedure in Nkede et al. (2024). TS and EAB were calculated using Eqs. (4) and (5):

$$\text{TS} = \frac{\text{Force at break}}{\text{Film thickness} \times \text{Width of film}} \quad (4)$$

$$\text{EAB}\ (\%) = \frac{\text{Final length of gap} - \text{Initial length of gap}}{\text{Initial length of gap}} \times 100 \quad (5)$$

2.4.12. Water vapor permeability (WVP)

WVP was measured following the method of Meng et al. (2026) with slight modifications. Permeability cups (8 cm diameter, 1 cm height) containing 5 g anhydrous calcium chloride were sealed with film samples and weighed. Cups (surface area: 0.0028 m²) were placed in a controlled humidity chamber at 20 °C and 70% RH ($\Delta P = 3169$ Pa). Weight gain was recorded every 2 h for 10 h, and WVP was calculated using Eq. (6). Measurements were performed in quadruplicate.

$$\text{WVP} = \frac{\text{Slope}}{\text{Film permeation area} \times \text{Water vapor pressure difference}} \times \text{Film thickness (m)} \quad (6)$$

2.4.13. Water contact angle

Surface wettability was evaluated using a Smart Contact Mobile Entry 2 analyzer (Exima Yokohama Lab Co., Ltd., Japan) following the protocol of Meng et al. (2025). A distilled

water droplet (~5 μL) was deposited on the film surface, and images were captured for analysis. Measurements were performed in triplicate to assess hydrophilic–hydrophobic balance within the film matrix.

2.4.14. Moisture content

Moisture content was determined using a modified method from Takahashi et al. (2024). Pre-dried aluminum pans were weighed, film samples (2 × 2 cm^2) were added, and the pans were dried at 105 °C for 24 h. MC was calculated using Eq. (7). Measurements were performed in quadruplicate.

$$\text{MC}\ (\%) = \frac{\text{Weight of films before drying} - \text{Weight of films after drying}}{\text{Weight of films before drying} - \text{Weight of pan after drying}} \times 100 \quad (7)$$

2.4.15. Thermogravimetric analysis (TGA)

Thermal stability was assessed using a TG/DTA7300 analyzer (Japan). Film samples (~3.8 mg) were heated from 30 to 500 °C at 20 °C min^{-1} under a nitrogen purge (300 mL min^{-1}), following the method from Nkede et al. (2024). Thermograms were used to evaluate degradation behavior and compositional transitions within the biopolymer matrix.

2.5. Application of edible coatings on blueberries

Blueberries were washed using distilled water, air-dried, and immersed in each coating formulation for 1 min, drained, and air-dried again before storage. Control fruits were treated with deionized water (Li et al. 2021). All samples were stored at 25 °C and 65% RH for 10 days to simulate commercial conditions, with quality parameters evaluated every 2 days. Visual assessments were conducted at each interval to monitor shriveling, color changes, and decay incidence.

2.6. Quality evaluation of stored blueberries

2.6.1. Weight loss

Weight loss was monitored throughout storage by recording fruit weight at each evaluation interval. Weight loss (%) was calculated using Eq. (8). This parameter reflected moisture loss and physiological deterioration.

$$\text{WL}\ (\%) = \frac{\text{Weight before storage} - \text{Weight during storage}}{\text{Weight before storage}} \times 100 \quad (8)$$

2.6.2. Surface color

Surface color was measured using a CR-20 colorimeter (Konica Minolta, Japan). CIE L*, *a**, and b* values were recorded at two equatorial positions per fruit, with three replicates per treatment, to assess color retention during storage.

2.6.3. Firmness

Firmness was measured using a creep meter (Rheoner II RE3 3305C, Yamaden Ltd., Japan) with a 4 mm probe, 30% deformation rate, 1 mm s^{-1} penetration speed, and 0.05 s data interval. Firmness was expressed as the force (N) required to penetrate the tissue. Three replicates per treatment were analyzed.

2.6.4. pH and Total soluble solids

Blueberry juice was prepared by homogenizing 1 g of fruit with 9 g distilled water and filtering through Whatman paper. A 400 µL aliquot was used for pH measurement (LAQUAtwin pH 22, Japan), and another 400 µL aliquot was analyzed using a digital refractometer (Atago, Japan) to determine total soluble solids (TSS, %). These parameters were used to track changes in sweetness and acidity associated with postharvest metabolism.

2.7. Statistical analysis

A completely randomized design (CRD) was used for all experiments. Treatment effects were analyzed using ANOVA, and significant differences were identified using Fisher's least significant difference (LSD) test at $p < 0.05$. All statistical analyses were performed in MINITAB (version 22), and results are expressed as mean ± standard deviation. Principal component analysis (PCA) was conducted using weight loss, color parameters, firmness, pH, and TSS to visualize multivariate patterns and treatment clustering. Pearson's correlation analysis was used to determine correlation coefficients (r) among blueberry quality attributes, providing insight into interrelationships among key postharvest indicators.

3. Results and discussion

3.1. Emulsion stability, zeta potential and oil binding capacity

The physical stability of the ultrasound-assisted SA/HA/CNF Pickering emulsions (PEs) was monitored for 8 days (Fig. 1A). All formulations maintained a uniform milky appearance without phase separation, oiling off, or creaming, indicating good physical stability (Nkede et al. 2024). Because all formulations contained HA, the present experimental design does not permit the independent contribution of HA to emulsion stability to be determined. Nevertheless, the formulation containing 0.5% HA showed a slight improvement in stability relative to the 0.2% HA formulation, which may be associated with differences in the hydrated polymeric environment and continuous-phase viscosity. The improved stability observed at the higher HA concentration may be related to the combined interfacial and bulk effects of HA within the CNF-stabilized system. HA contains abundant hydrophilic groups that can associate strongly with water and may increase hydration of the interfacial region

(Wang et al. 2026). Hydrated HA chains may also provide steric protection around the droplets and modify the viscosity of the continuous phase, potentially reducing droplet mobility and collision frequency. Together with CNF adsorption at the oil–water interface, these effects may contribute to the physical stability observed in the HA-containing formulations.

The zeta-potential values ranged from −40.13 to −82.87 mV, indicating substantial electrostatic repulsion among the dispersed droplets. The relatively high absolute values may have contributed to the observed physical stability of the emulsions. The more negative zeta-potential values further suggest that electrostatic repulsion may have contributed to limiting close approach between droplets. Because formulations without HA were not included and interfacial rheology and droplet-size measurements were not performed, these interpretations should be considered mechanistic possibilities rather than direct evidence of the independent stabilizing role of HA. Consistent with these findings, previous studies have reported decreased zeta potential upon essential oil incorporation into coating systems (Bibi et al. 2026a). The ultrasound treatment used during emulsification may have contributed to efficient dispersion of the oil phase by generating cavitation-associated shear and promoting interactions among the oil droplets and CNF-based stabilizing phase (Liu et al. 2025). Such processing could facilitate the formation of smaller or more uniformly distributed droplets and improve contact between the dispersed phase and interfacial stabilizers (Cheng et al. 2024). However, the present experimental design does not allow the specific contribution of ultrasound to be separated from the effects of CNF and HA functionalization because a corresponding non-ultrasound control was not included. Therefore, the observed stability

should be interpreted as a property of the ultrasound-assisted HA-functionalized CNF Pickering emulsion rather than as direct evidence of ultrasound-induced enhancement. The improved stability observed with increasing HA concentration may be related to the combined interfacial and bulk effects of HA within the CNF-stabilized system. HA contains abundant hydrophilic groups that can strongly associate with water and may increase the hydration of the interfacial region (Cao et al. 2026). In addition, the hydrated HA chains may provide steric protection around the droplets and increase the viscosity of the continuous phase, thereby reducing droplet mobility and the probability of collision and coalescence. Together with the interfacial adsorption of CNF, these effects may contribute to the greater physical stability observed for the HA-containing formulations. The more negative zeta-potential values further suggest that electrostatic repulsion may have contributed to limiting close approach between droplets. Because interfacial rheology and droplet-size measurements were not performed, however, these mechanisms remain interpretative rather than directly demonstrated.

The oil-binding capacity ranged from 1.25 to 1.95 g/g, with SA/0.5 HA-PE showing the highest value (Fig. 1C). The greater oil retention observed at the higher HA concentration may be associated with increased hydration and viscosity of the polymeric continuous phase and improved physical entrapment of the dispersed oil phase (Guo et al. 2022). The presence of PE droplets may further strengthen interactions between the oil phase and the polymer matrix, increasing the films' affinity for oil retention (Ma et al. 2023). Similar enhancements have been reported in HA-based films containing oleogels (Cao et al. 2026).

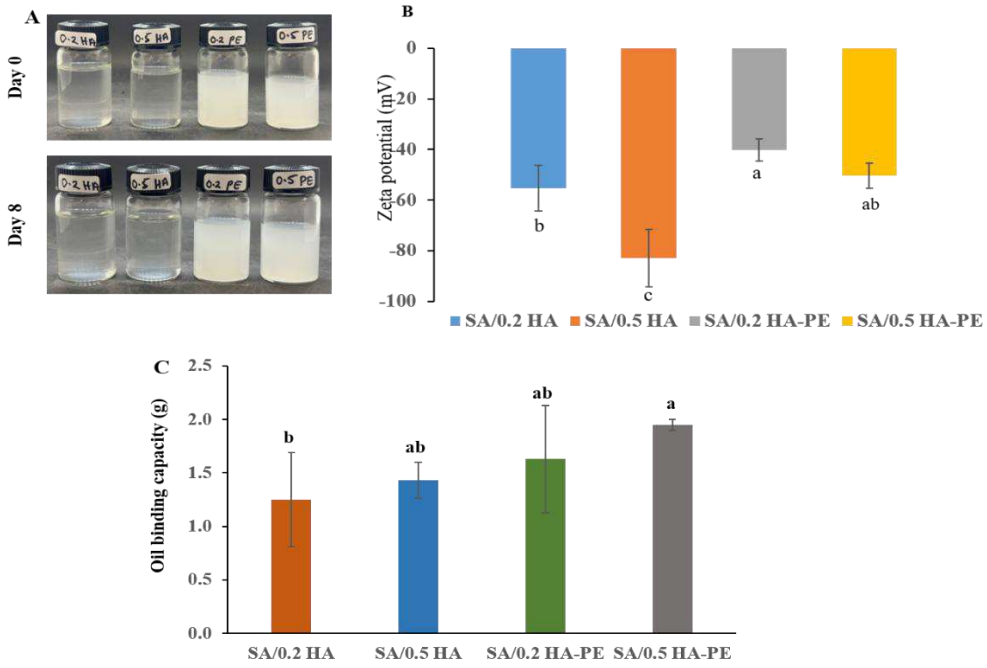


Fig. 1. Emulsion stability **(A),** zeta potential **(B),** and oil binding capacity (C) of coating samples.

3.1.1. Visual Appearance and color properties of the prepared films

All film formulations (SA/0.2 HA, SA/0.5 HA, SA/0.2 HA-PE, and SA/0.5 HA-PE) produced continuous, smooth, and transparent films without cracks, pores, or visible phase separation. The underlying image remained clearly visible through each film (Fig. 2), consistent with their high L* values (>95) and low ΔE values (Table 1). Incorporation of the PEO-PE did not affect film clarity, and no droplet aggregation was observed, indicating good dispersion of the emulsion within the SA–HA matrix. The uniform appearance of PE-containing films reflects strong compatibility among SA, HA, CNF, and PEO, aligning with FTIR results showing only minor spectral shifts associated with intermolecular interactions. Overall, both HA and the Pickering emulsion were successfully integrated into the polymer network without compromising visual quality—an essential requirement for edible coatings and food-packaging applications.

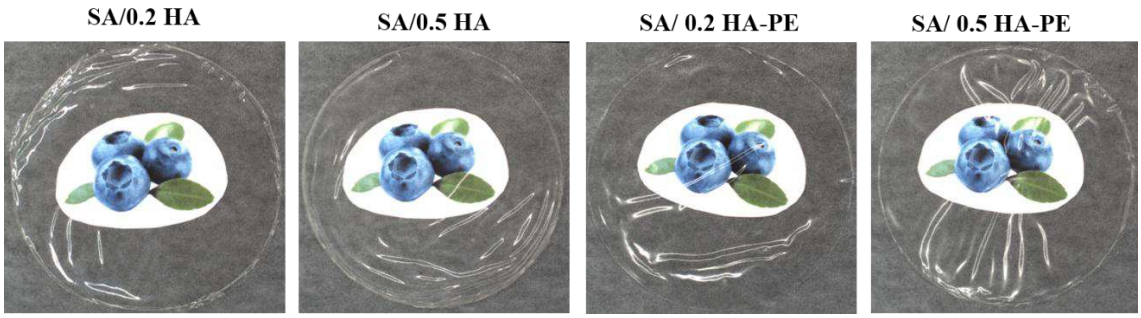


Fig. 2. Appearance of SA/0.2 HA, SA/0.5 HA, SA/0.2 HA-PE, and SA/0.5 HA-PE films.

Color measurements supported the visual observations. All films showed high lightness, with L* values of 95.82–96.52 (Table 1), indicating bright, uniform surfaces. Although L* differences were statistically significant ($p < 0.05$), the small variation suggests that neither HA concentration nor PE incorporation meaningfully affected brightness. The *a** values (0.24–0.28) did not differ significantly ($p > 0.05$), confirming similar red–green characteristics across formulations. In contrast, b* values varied significantly ($p < 0.05$). Films containing the PE exhibited higher yellowness (6.23–6.27) than SA/HA films (5.50), likely due to natural pigments and volatile constituents in parsley essential oil (Wong and Kitts 2006b). Total color difference (ΔE) values ranged from 2.72 to 3.01, with SA/0.5 HA-PE showing the highest ΔE ($p < 0.05$). Comparable increases in ΔE have been reported when essential oils or Pickering emulsions are incorporated into polymer matrices (Montes-Ramírez et al. 2024; Nkede et al. 2023a). Despite these differences, all ΔE values remained low, indicating that the films maintained acceptable transparency and visual quality (Fig. 2). Film opacity increased from 2.77 ± 0.08 in SA/0.2 HA to 3.56 ± 0.03 in SA/0.5 HA-PE (Table 1), with emulsified films consistently showing higher opacity than non-emulsified ones. Both higher HA concentration and PE incorporation contributed to this increase, although the emulsion effect was more pronounced. This trend aligns with observations in

cellulose-nanofiber-stabilized lemongrass oil Pickering films, where emulsion addition significantly enhanced opacity (Nkede et al. 2023b). The increase is primarily attributed to light scattering by dispersed oil droplets and interfacial stabilizers (Wardana et al. 2021).

Table 1. Color properties and opacity of the film samples.

Parameters	SA/0.2 HA	SA/0.5 HA	SA/0.2 HA-PE	SA/0.5 HA-PE
L*	96.05 ± 0.55^{ab}	96.52 ± 0.34^{a}	95.82 ± 0.29^{b}	96.23 ± 0.33^{ab}
a*	0.25 ± 0.035^{a}	0.24 ± 0.07^{a}	0.28 ± 0.02^{a}	0.27 ± 0.03^{a}
b*	6.00 ± 0.16^{a}	5.50 ± 0.44^{b}	6.23 ± 0.19^{a}	6.27 ± 0.15^{a}
ΔE	2.72 ± 0.24^{b}	2.74 ± 0.07^{b}	2.74 ± 0.08^{b}	3.01 ± 0.13^{a}
Opacity	2.77 ± 0.08^{c}	3.00 ± 0.16^{bc}	3.31 ± 0.44^{ab}	3.56 ± 0.03^{a}

Means with different letters (a, b, c) on the same row indicate significant differences ($p < 0.05$) according to Fisher's LSD test.

3.1.2. Thickness, MC, WVP, WCA, and mechanical properties of the film samples

Film thickness ranged from 0.042 to 0.061 mm and differed significantly among formulations ($p < 0.05$). SA/0.2 HA produced the thinnest films, whereas SA/0.5 HA-PE was the thickest (Table 2). Increasing HA concentration from 0.2% to 0.5% led to thicker films, likely due to the higher solid content and viscosity of the film-forming solution—an effect commonly reported for polysaccharide systems (Sgorla et al. 2016a). Incorporation of the PEO-PEs further increased thickness, as dispersed oil droplets contributed internal volume and promoted a more structured polymer network (Shen et al. 2021; Xu et al. 2020). The pronounced increase in SA/0.5 HA PE suggests a synergistic effect between higher HA content and emulsion addition. These structural changes align with FTIR observations (Fig. 4), where shifts in the O–H stretching region indicated strengthened intermolecular interactions that likely enhanced network cohesion and solid retention during drying.

391 Moisture content (MC) ranged from 10.17% to 12.93% (Table 1), with no significant
392 differences among formulations ($p > 0.05$). Films containing 0.5% HA showed slightly
393 higher MC than those with 0.2% HA, consistent with HA's strong water-binding capacity and
394 abundance of hydrophilic functional groups (Sgorla et al. 2016). Incorporation of the PEO
395 Pickering emulsion did not significantly alter MC, indicating that the hydrophobic oil phase
396 did not disrupt the moisture-retention behavior of the SA–HA matrix. The similar MC values
397 across all formulations suggest stable interactions between the hydrophilic polymer network
398 and dispersed emulsion droplets. This stability aligns with FTIR observations showing
399 predominantly physical interactions and good compatibility among sodium alginate,
400 hyaluronic acid, and the Pickering emulsion components.
401 Water vapor permeability (WVP) is a key barrier property for fruit packaging, as low
402 permeability limits moisture transfer between produce and its environment. In this study,
403 WVP differed significantly among formulations ($p < 0.05$), ranging from 7.14×10^{-4} to
404 8.86×10^{-4} g·m/m²·h·Pa (Table 2). The SA/0.5 HA film showed the highest WVP
405 (8.86×10^{-4} g·m/m²·h·Pa), whereas SA/0.5 HA-PE exhibited the lowest
406 (7.14×10^{-4} g·m/m²·h·Pa). Increasing HA concentration from 0.2% to 0.5% (without
407 emulsions) increased WVP, consistent with HA's strong hydrophilicity and abundance of
408 hydroxyl and carboxyl groups that readily bind water molecules (Sgorla et al. 2016). This
409 trend corresponds with the lower water contact angles observed for more hydrophilic films,
410 reflecting greater availability of polar groups for water adsorption and diffusion.
411 Incorporation of the PEO Pickering emulsion altered the barrier behavior. Although the
412 SA/0.2 HA-PE film still exhibited a relatively high WVP (8.63×10^{-4} g·m/m²·h·Pa), the

SA/0.5 HA-PE film showed a marked reduction compared with all other formulations. This trend aligns with the lower water contact angles observed for more hydrophilic films, indicating greater availability of polar groups for water adsorption and diffusion. Incorporation of the PEO Pickering emulsion modified the barrier behavior. This improvement likely reflects the combined effects of the hydrophobic essential-oil phase, increased film thickness, and enhanced intermolecular interactions among SA, HA, and emulsion droplets, as supported by FTIR observations (Fig. 4). The dispersed oil droplets, together with higher HA content, likely introduced a more tortuous diffusion pathway that restricted moisture transfer through the film et al. 2023a; Wigati et al. 2023).

Water contact angle (WCA) values ranged from 43.91° to 73.14° and were significantly affected by film composition ($p < 0.05$). The SA/0.2 HA film showed the lowest WCA, indicating a highly hydrophilic surface. Increasing HA concentration to 0.5% raised WCA to 65.55° (Table 2; Supplementary Fig. S1), reflecting reduced wettability. Incorporation of the PE further increased hydrophobicity, with SA/0.2 HA-PE exhibiting the highest WCA (73.14°), consistent with the presence of hydrophobic essential-oil droplets that limit surface-exposed polar groups—a trend also observed in polysaccharide films containing lipid phases (Wigati et al. 2023). Interestingly, SA/0.5 HA-PE displayed a lower WCA (57.88°) than SA/0.2 HA-PE. This reduction likely reflects the higher proportion of hydrophilic hydroxyl and carboxyl groups contributed by HA, which interact readily with water (Al-Hilifi et al. 2024). Overall, surface wettability appears governed by the balance between hydrophobic essential-oil domains and hydrophilic polysaccharide components. Improved moisture-barrier performance has practical implications beyond material functionality.

435 Reduced water vapor transmission slows dehydration, thereby decreasing food losses during
436 storage and distribution. From a cleaner-production perspective, extending product shelf life
437 contributes to lower resource consumption across the food supply chain by reducing the
438 frequency of product replacement and minimizing waste generation.
439 Biopolymer films used in food packaging require adequate tensile strength (TS) and
440 flexibility to withstand handling and storage (Mai et al. 2025). The TS and elongation at
441 break (EAB) values of sodium alginate–hyaluronic acid (SA–HA) films containing parsley
442 essential oil Pickering emulsions are shown in Table 2. Film composition significantly
443 affected TS ($p < 0.05$), whereas EAB did not vary among formulations ($p > 0.05$). TS ranged
444 from 95.50 to 136.56 MPa, with SA/0.5 HA exhibiting the highest strength (136.56 MPa),
445 significantly greater than SA/0.2 HA (102.73 MPa) and SA/0.2 HA-PE (95.50 MPa). The TS
446 enhancement at higher HA levels reflects matrix reinforcement through intensified
447 intermolecular interactions. HA's hydroxyl and carboxyl groups promote hydrogen bonding
448 with alginate, strengthening chain cohesion (Liu et al. 2013; Mai et al. 2025), consistent with
449 FTIR shifts in the O–H region. Similar HA-induced reinforcement has been reported in
450 carboxymethyl cellulose films (Kim et al. 2020). Incorporating the parsley essential oil
451 Pickering emulsion slightly reduced TS, likely because dispersed oil droplets act as structural
452 discontinuities that interrupt polymer–polymer interactions (Nkede, Wardak, Wardana, et al.
453 2024b). TS decreased from 136.56 to 116.72 MPa in SA/0.5 HA-PE and from 102.73 to
454 95.50 MPa in SA/0.2 HA-PE, a trend comparable to essential-oil-loaded HA films (El-Aassar
455 et al. 2021). Nevertheless, SA/0.5 HA-PE retained relatively high strength, indicating that
456 the reinforcing effect of higher HA content partly compensated for emulsion-induced

457 weakening. The homogeneous film appearance (Fig. 2) suggests uniform emulsion
458 dispersion, minimizing structural defects. EAB values (4.35–6.04%) showed no significant
459 differences ($p > 0.05$). Although emulsified films displayed slight numerical increases in
460 EAB, these changes were not statistically meaningful, indicating that neither HA
461 concentration nor emulsion incorporation substantially affected flexibility. The combination
462 of maintained EAB and relatively high TS demonstrates a favorable balance between strength
463 and extensibility, suitable for edible coating applications. Overall, increasing HA
464 concentration effectively reinforced the SA matrix through enhanced intermolecular
465 interactions, while the ultrasound-engineered Pickering emulsion was incorporated without
466 compromising film flexibility.

467 **Table 2.** Thickness, water contact angle (WCA), water vapor permeability (WVP), moisture content
468 (MC), tensile strength (TS), and elongation at break (EAB) of the film samples.

Parameters	SA/0.2 HA	SA/0.5 HA	SA/0.2 HA-PE	SA/0.5 HA-PE
Thickness (mm)	0.042 ± 0.002^{c}	0.053 ± 0.004^{b}	0.055 ± 0.001^{b}	0.061 ± 0.005^{a}
WCA	43.91 ± 6.00^{c}	65.55 ± 5.47^{ab}	73.14 ± 13.79^{a}	57.88 ± 0.73^{bc}
WVP ($\times 10^{-4}$ g·m/m²·h·Pa)	7.75 ± 0.47^{bc}	8.86 ± 0.96^{a}	8.63 ± 0.33^{ab}	7.14 ± 0.42^{c}
MC (%)	10.55 ± 0.56^{a}	12.93 ± 1.20^{a}	12.61 ± 1.13^{a}	10.17 ± 2.44^{a}
TS (MPa)	102.73 ± 22.16^{b}	136.56 ± 14.60^{a}	95.50 ± 27.39^{b}	116.72 ± 18.96^{ab}
EAB (%)	5.41 ± 2.33^{a}	4.35 ± 1.25^{a}	6.04 ± 1.57^{a}	5.97 ± 1.07^{a}

469 Means with different letters (a, b, c) on the same row indicate significant differences ($p < 0.05$)
470 according to Fisher's LSD test.

471 **3.1.3. Confocal Laser Scanning Microscopy (CLSM)**

472 Confocal laser scanning microscopy (CLSM) was used to visualize the distribution of parsley
473 essential-oil Pickering emulsion droplets within the SA–HA films, with Nile Red labeling
474 the oil phase (Fig. 3). The 2D images showed uniformly dispersed droplets in both

SA/0.2 HA-PE and SA/0.5 HA-PE films, with no aggregation or phase separation. The 3D reconstructions confirmed homogeneous embedding of CNF–HA-stabilized droplets, demonstrating successful incorporation of the Pickering emulsion (J. Zhang et al. 2026). This uniformity aligns with expected molecular interactions—such as entrapment and hydrogen bonding between polysaccharides and essential-oil components (Xu et al. 2019). Compared with SA/0.2 HA-PE, the SA/0.5 HA-PE film exhibited a more homogeneous distribution. The more homogeneous fluorescence distribution observed for SA/0.5 HA-PE may be associated with improved stabilization of the dispersed oil phase within the HA–CNF–SA matrix (Wang et al. 2026). CNF can adsorb at the oil–water interface and form a physical barrier around droplets, while hydrated HA chains may provide additional steric stabilization and modify the local viscosity of the continuous phase. These combined effects could reduce droplet aggregation during incorporation into the alginate matrix and contribute to the more uniform microstructure observed by CLSM. Nevertheless, direct droplet-size and interfacial-rheology measurements would be required to verify this proposed mechanism.

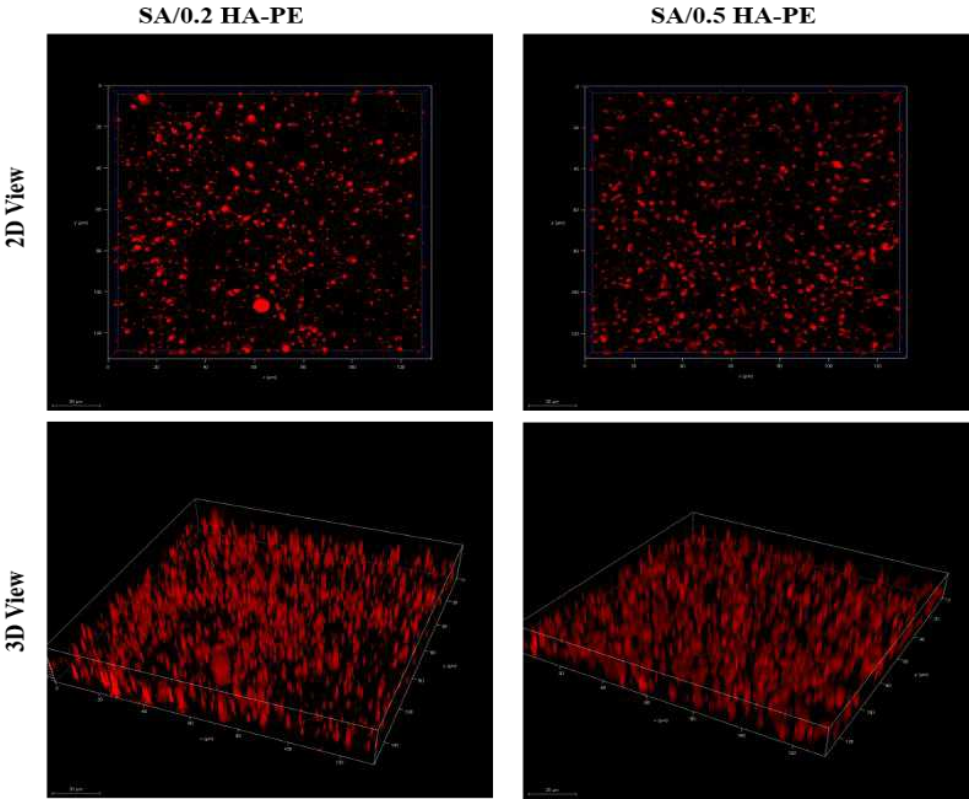


Fig. 3. Confocal laser scanning microscopy (CLSM) 2D and 3D images of SA/0.2 HA-PE and SA/0.5 HA-PE films stained with Nile Red, showing the distribution of parsley essential oil Pickering emulsion droplets within the sodium alginate–hyaluronic acid matrix.

3.1.4. Scanning Electron Microscopy (SEM)

SEM micrographs of SA/0.2 HA, SA/0.5 HA, SA/0.2 HA-PE, and SA/0.5 HA-PE films (Fig. 4) revealed continuous, compact structures across all formulations, with no cracks, pores, or phase separation. This uniform morphology indicates strong compatibility among sodium alginate, hyaluronic acid, and the Pickering-emulsion components. Control films displayed smooth, homogeneous surfaces, whereas PE-containing films showed slightly rougher textures attributable to dispersed parsley essential-oil droplets. Importantly, no droplet aggregation or oil leakage was observed, confirming effective dispersion of the CNF–

HA-stabilized emulsion within the polymer matrix. These observations align with Liu et al. (2026), who reported that hyaluronic acid promotes dense, continuous matrices without phase separation when essential oils are incorporated. Cross-sectional images further confirmed compact internal structures, with SA/0.5 HA-PE exhibiting a denser and thicker morphology—consistent with its higher measured thickness and lower water-vapor permeability. The compact morphology observed for the PE-containing films may reflect the combined contribution of the alginate–HA polymer network and the dispersed Pickering-emulsion phase. The absence of large pores, cracks, or obvious phase separation suggests good physical compatibility among the coating components. The denser appearance of SA/0.5 HA-PE is also consistent with the higher HA concentration and greater oil-binding capacity observed for this formulation.

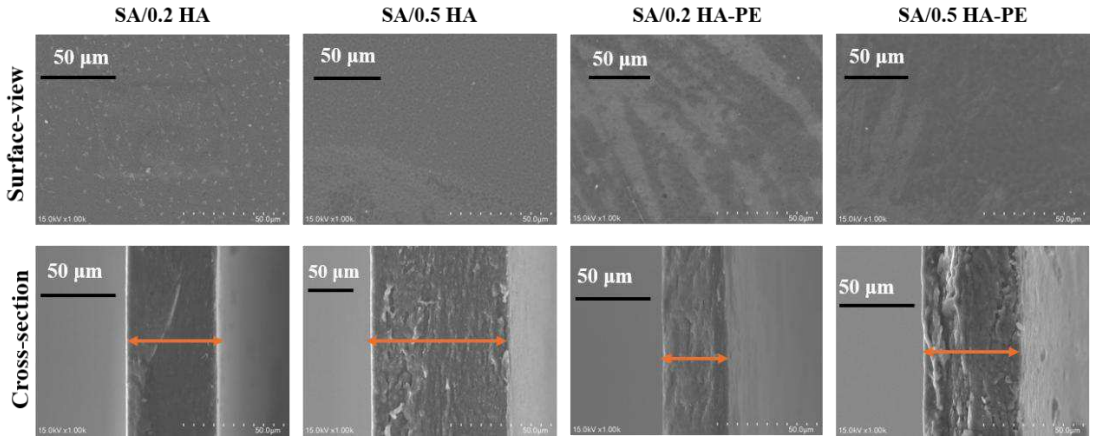


Fig. 4. Surface and cross-sectional scanning electron microscopy (SEM) micrographs of SA/0.2 HA, SA/0.5 HA, SA/0.2 HA-PE, and SA/0.5 HA-PE films.

3.1.5. Fourier Transform Infrared Spectroscopy (FTIR)

FTIR spectra of SA/0.2 HA, SA/0.5 HA, SA/0.2 HA-PE, and SA/0.5 HA-PE films (Fig. 5) showed the characteristic bands of the sodium alginate–hyaluronic acid matrix, indicating that neither HA nor the parsley essential-oil Pickering emulsion introduced new functional

518 groups or altered the polymer backbone. Instead, the spectra reflected noncovalent
519 interactions among components. The broad O–H stretching band at 3261–3288 cm^{-1}
520 corresponded to hydroxyl groups in SA, HA, glycerol, and bound water (Nkede et al. 2024b;
521 Wardak et al. 2024; Zhou et al. 2024). Increasing HA concentration shifted this band to higher
522 wavenumbers, suggesting strengthened hydrogen bonding within the polymer network. After
523 PE incorporation, slight shifts to lower wavenumbers indicated enhanced hydrogen bonding
524 between polysaccharide chains and emulsion droplets (Wang et al. 2024). Symmetric and
525 asymmetric C–H stretching vibrations (2875–2885 cm^{-1}; 2929–2937 cm^{-1}) appeared in all
526 films, with small upward shifts reflecting subtle changes in aliphatic group environments due
527 to modified chain packing (Al-Hilifi et al. 2024; Sgorla et al. 2016). The asymmetric COO^{-}
528 stretching band at 1598.70 cm^{-1} shifted slightly after PE incorporation (1600.63 and
529 1594.84 cm^{-1}), indicating weak hydrogen bonding or electrostatic interactions between
530 carboxyl groups and emulsion droplets (Liu et al. 2025). Minor shifts in the C–O–C/C–OH
531 region (1403–1408 cm^{-1}) further reflected changes in chain organization (Liu et al. 2026;
532 Nkede et al. 2023; Zhou et al. 2024). Overall, the absence of new absorption bands and the
533 presence of relatively small peak shifts are consistent with physical incorporation of the
534 Pickering emulsion and predominantly noncovalent interactions within the composite matrix.
535 Hydrogen bonding and electrostatic interactions may contribute to the observed changes in
536 the spectral positions of characteristic functional groups, while physical entrapment may
537 facilitate retention of the emulsion droplets within the SA–HA network (Zhang et al. 2024).

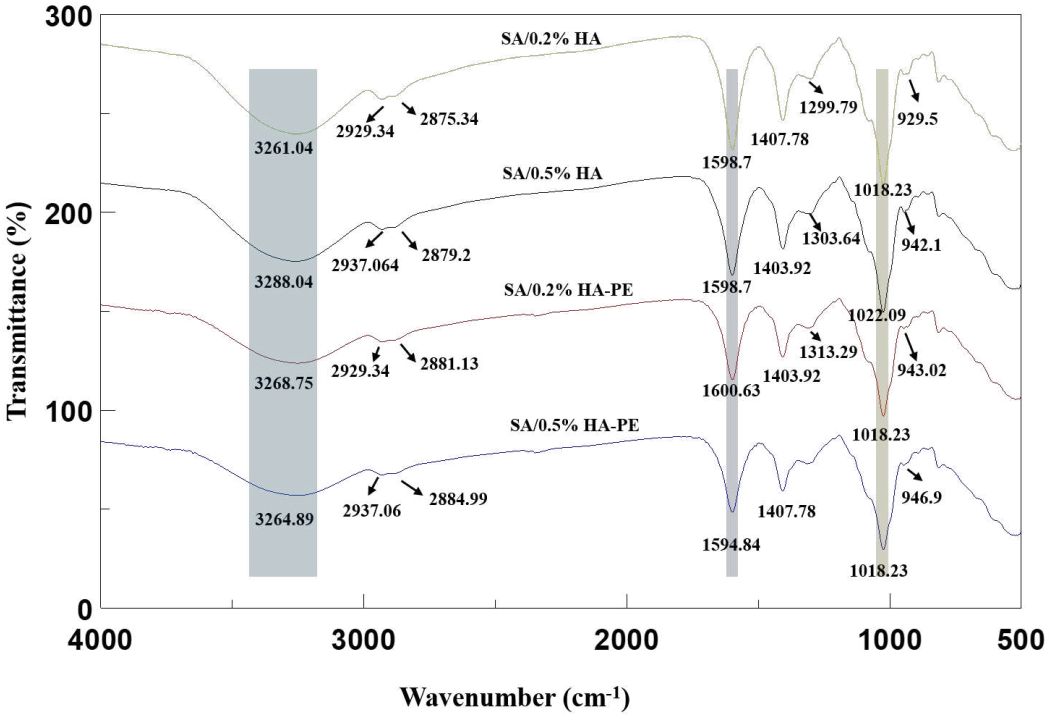


Fig. 5. FTIR spectra of SA/0.2% HA, SA/0.5% HA, SA/0.2% HA-PE, and SA/0.5% HA-PE films.

3.1.6. UV–visible light transmittance

The UV–visible transmittance spectra of SA/0.2 HA, SA/0.5 HA, SA/0.2 HA-PE, and SA/0.5 HA-PE films (Fig. 6) showed that all formulations almost completely blocked UVC radiation (200–280 nm), reflecting the strong intrinsic UV-absorbing capacity of the polysaccharide matrix. Transmittance increased in the UVB (280–320 nm) and UVA (320–400 nm) regions and remained stable across the visible range (400–800 nm), where values of ~55–75% indicated good transparency—consistent with visual observations (Fig. 2). This level of visible-light transmittance is desirable for edible coatings and packaging, where product visibility is important. Incorporation of the parsley essential-oil Pickering emulsion reduced transmittance, particularly in the UVA and visible regions. This reduction likely resulted from increased light scattering by dispersed emulsion droplets and

absorption/scattering by phenolic and terpenoid compounds naturally present in parsley essential oil. The lower transmittance of SA/0.5 HA-PE suggests that the combined effects of higher HA concentration and PE incorporation enhanced light-barrier performance. Overall, the results indicate that adding the Pickering emulsion improved UV shielding while maintaining adequate transparency for active edible-coating applications. Similar enhancements in UV-blocking performance have been reported for films containing Pickering emulsions (Nkede et al. 2023a; Zhang et al. 2024)

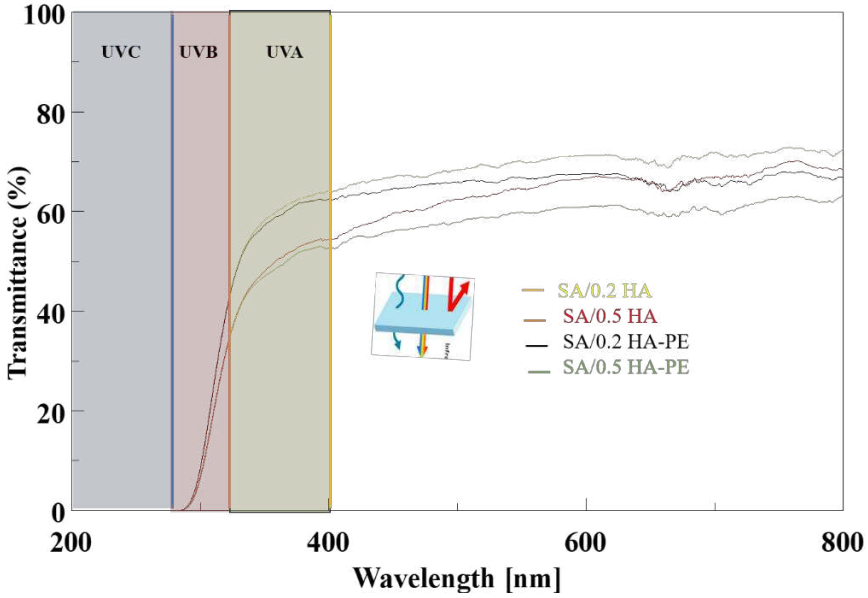
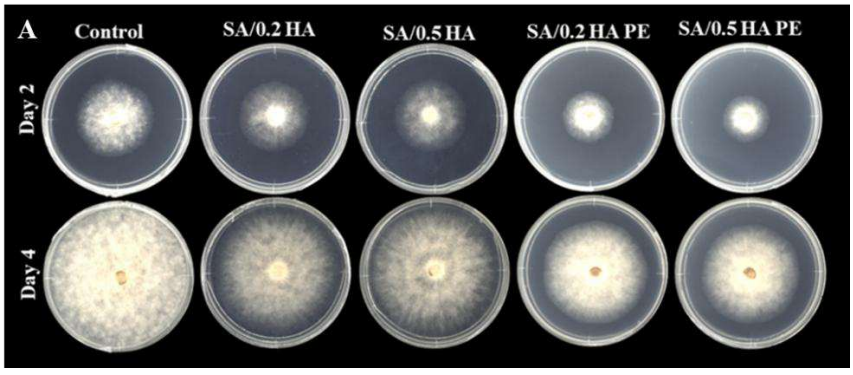


Fig. 6. UV-visible transmittance spectra of the SA/0.2% HA, SA/0.5% HA, SA/0.2% HA-PE, and SA/0.5% HA-PE films.

3.1.7. Antifungal Activity

The antifungal activity of the coating formulations against *Botrytis cinerea* (Fig. 7) showed that all coatings inhibited fungal growth relative to the control, with the strongest effects observed in formulations containing the parsley essential-oil Pickering emulsion. After 2 days of incubation, both SA/0.2 HA-PE and SA/0.5 HA-PE significantly reduced mycelial

566 expansion compared with the other treatments ($p < 0.05$). Although colony size increased
567 after 4 days, the Pickering-emulsion coatings consistently maintained smaller diameters than
568 the control and the corresponding non-emulsified coatings. Among all formulations,
569 SA/0.5 HA-PE exhibited the most pronounced antifungal activity throughout the incubation
570 period. The stronger inhibition observed for the PE-containing coatings is likely associated
571 with the bioactive constituents of parsley essential oil, which have been reported to interfere
572 with fungal membrane integrity and cellular metabolism. Incorporation of the oil into the
573 CNF–HA Pickering emulsion may have improved its dispersion within the coating matrix
574 and potentially influenced the availability of its active constituents at the film–environment
575 interface (Staropoli et al. 2021; Živković et al. 2026). The higher oil-binding capacity and
576 compact microstructure observed for the PE-containing films are consistent with this
577 interpretation.



578

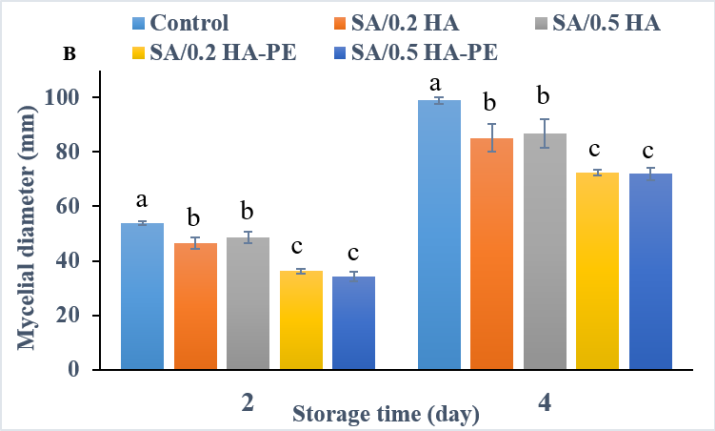
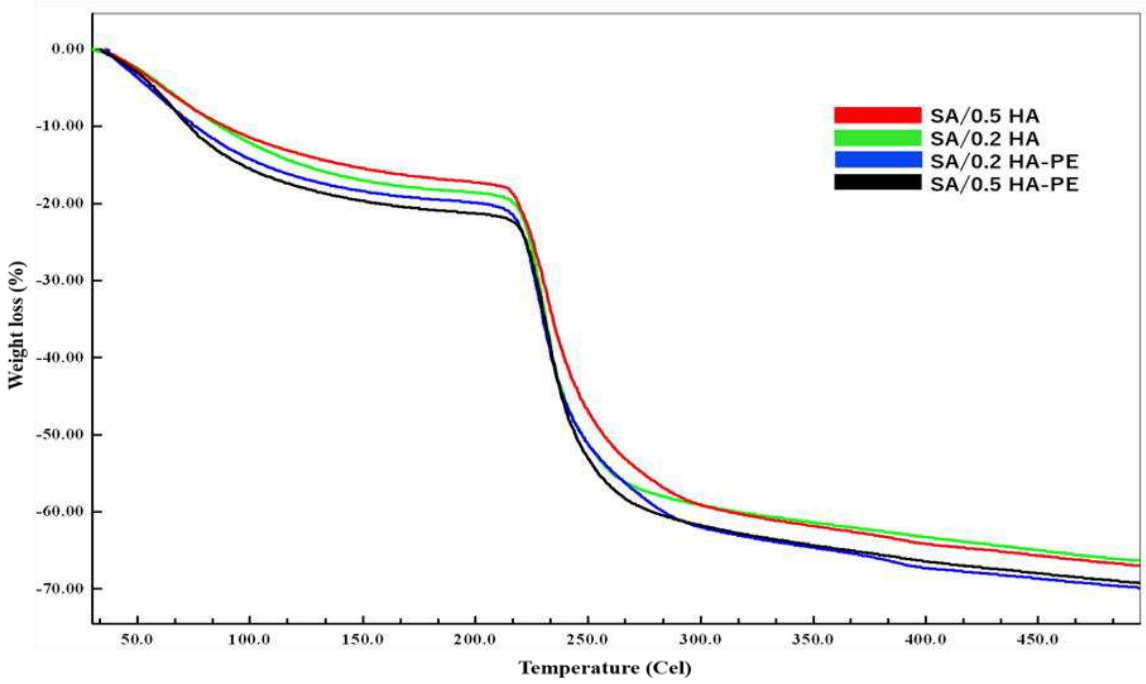


Fig. 7. Antifungal activity of sodium alginate–hyaluronic acid coatings with and without parsley essential oil Pickering emulsion against *Botrytis cinerea*.

3.1.8. Thermogravimetric Analysis (TGA)

The thermal stability of the sodium alginate–hyaluronic acid composite films was evaluated using thermogravimetric analysis (Fig. 8). All formulations exhibited the characteristic multi-stage thermal degradation behavior typical of polysaccharide-based materials. The first degradation stage occurred between approximately 35 and 201 °C and corresponded to the evaporation of free and bound water as well as low-molecular-weight volatile compounds (Abbaszadeh et al. 2025; Alemdar 2016; Wardak et al. 2024). Weight loss during this stage ranged from 17.3% to 21.1%, with the SA/0.5 HA-PE film showing the highest initial mass loss. The major degradation stage occurred between roughly 180 and 346 °C and was attributed to decomposition of the sodium alginate–hyaluronic acid polymer network through cleavage of glycosidic linkages and breakdown of the polysaccharide backbone (Abbaszadeh et al. 2025). The SA/0.5 HA and SA/0.2 HA-PE films exhibited a distinct second degradation event, whereas this stage overlapped with the final degradation phase in SA/0.2 HA and SA/0.5 HA-PE, resulting in a two-stage degradation profile. The final degradation stage

595 extended to approximately 492 °C and was associated with decomposition of the remaining
596 carbonaceous residues (Nkede et al. 2024b). Despite minor differences in degradation
597 patterns among the formulations, all films demonstrated good thermal stability across a broad
598 temperature range. Importantly, incorporation of the CNF–HA-stabilized parsley essential oil
599 Pickering emulsion did not negatively affect thermal stability, indicating strong compatibility
600 between the emulsion droplets and the sodium alginate matrix. This observation is consistent
601 with FTIR results, which showed that film components interacted primarily through
602 intermolecular interactions rather than formation of new covalent bonds. Similar findings
603 were reported by (Liu et al. 2026), who observed that adding carvacrol or carvacrol-loaded
604 β-cyclodextrin did not alter the thermal decomposition peaks of GE/HA composite films,
605 suggesting that such bioactive additives do not compromise thermal stability.



606 **Fig. 8.** TGA of SA/0.2 HA, SA/0.5 HA, SA/0.2 HA-PE, and SA/0.5 HA-PE films.

607

3.2. Postharvest quality of uncoated and coated blueberries

3.2.1. Visual quality, weight loss, and firmness changes of blueberries during storage

The visual progression of blueberries during storage clearly illustrates the protective effect of the SA/HA coatings, particularly when reinforced with the Pickering emulsion (PE). By day 6, the control berries exhibited pronounced shriveling, surface dullness, and early softening—typical symptoms of rapid moisture loss and structural degradation in uncoated fruit. In contrast, berries treated with SA/0.2 HA and SA/0.5 HA maintained a more hydrated appearance and better skin integrity, although slight wrinkling became evident as storage advanced (Fig. 9A). The greatest improvement was observed in the SA/0.2 HA PE and SA/0.5 HA PE treatments, which retained a fresher appearance and firmer structure even by day 10. These berries showed minimal shriveling and preserved their natural bloom, indicating that PE-reinforced coatings provided a more effective barrier against moisture loss and oxidative changes.

Weight loss is a critical determinant of blueberry marketability with >8% loss often rendering fruit unacceptable (Mohamed and Ramaswamy, 2025). Weight loss increased progressively across all treatments. The control berries consistently exhibited the highest weight loss, rising from 3.66% on day 2 to 13.30% by day 10 (Fig. 9B). The PE- coatings showed lower weight loss of 8.07–8.42%. The lower water-vapor permeability observed for the PE-containing coatings, particularly SA/0.5 HA-PE, may have contributed to the reduced weight loss of the coated blueberries by limiting moisture transfer through the coating. This interpretation is consistent with the lower weight loss observed in the PE-treated fruit during storage. However, WVP alone cannot fully explain fruit weight loss because postharvest mass loss is

630 also influenced by physiological processes, including transpiration and respiration. Thus, the
631 association between the lower WVP of the coatings and reduced fruit weight loss should be
632 interpreted as evidence that improved moisture-barrier properties may have contributed to
633 preservation rather than as proof of a single controlling mechanism (Ji et al., 2026)
634 Comparable reductions in weight loss have been reported for blueberries coated with
635 chitosan–thyme essential oil Pickering emulsions (Wang et al., 2026).
636 Firmness followed an inverse trend relative to weight loss, underscoring the physiological
637 linkage between these attributes. Control berries softened rapidly, declining from 2.97 N at
638 day 0 to 1.34 N by day 10 (Fig. 9C), consistent with high transpiration-driven water loss. All
639 coated treatments slowed firmness decline, with PE-reinforced coatings showing the most
640 pronounced effect. From day 4 onward, SA/0.2 HA PE and SA/0.5 HA PE maintained
641 firmness values above 2.3 N, whereas the control dropped below 2.1 N. By day 10, coated
642 berries retained firmness values between 2.10 and 2.45 N, demonstrating better structural
643 integrity. The negative correlation between weight loss and firmness suggests that treatments
644 limiting moisture loss may also contribute to the retention of fruit structural integrity.
645 Reduced dehydration could help maintain cellular turgor and thereby delay softening.
646 Nevertheless, blueberry firmness is also influenced by enzymatic and structural changes in
647 cell-wall polysaccharides (Ding et al., 2024b; Jiang et al., 2023), so the observed relationship
648 should not be interpreted as evidence that moisture loss alone controlled firmness changes.

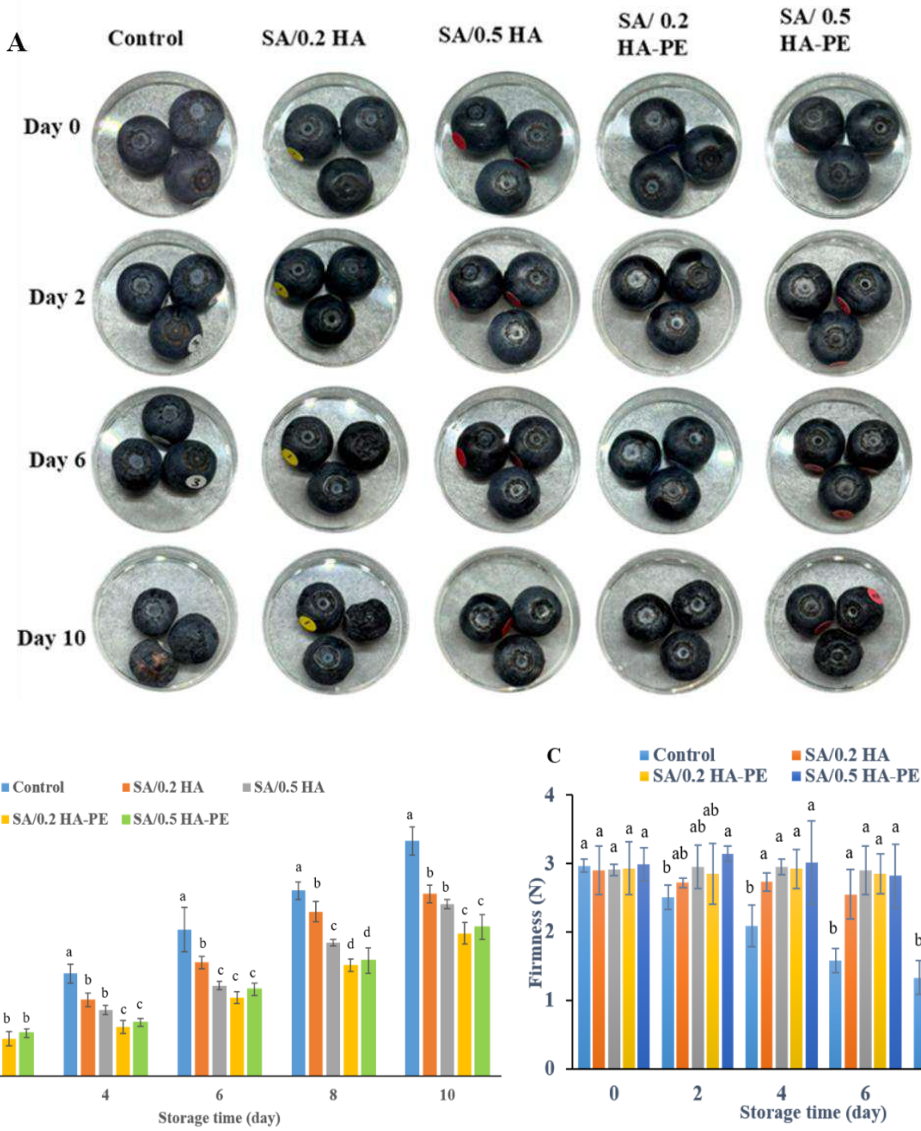


Fig. 9. Visual appearance (**A**), weight loss (**B**), and firmness (**C**) of blueberries under different coating treatments from day 0 to day 10.

3.2.2. Changes in color parameters

Color is a key quality attribute influencing consumer acceptance of fresh blueberries. In this study, L* represented fruit brightness, *a** indicated red–green coloration (with negative values corresponding to green), and b* reflected yellow–blue coloration (with negative values corresponding to blue). Throughout storage, coated blueberries generally maintained

color characteristics comparable to the control, although significant differences among treatments were observed ($p < 0.05$). The L* values increased during the early storage period and declined toward the end. The SA/0.5 HA treatment exhibited the highest lightness, reaching 31.15 on day 4 and maintaining a relatively high value (27.23) on day 10 (Table 3). In contrast, the SA/0.2 HA-PE treatment consistently showed lower L* values (21.93–27.43), indicating a darker fruit surface. These variations may be associated with differences in coating thickness and light scattering effects introduced by HA and parsley essential oil. Decreased brightness during storage is commonly linked to chlorophyll degradation (Das et al. 2022), progressive ripening and pigment accumulation, or enzymatic browning reactions involving polyphenol oxidase and phenolic substrates (Fei et al., 2026). The *a** values remained close to zero (−0.52 to 0.60), indicating minimal changes in the red–green component. Similarly, b* values remained negative across all treatments (−5.42 to −2.80), reflecting the characteristic blue coloration of blueberries. Although coated fruits—particularly those containing parsley essential oil showed slightly less negative b* values than the control, overall color was well preserved. These findings suggest that the HA-reinforced sodium alginate coatings effectively minimized pigment degradation and delayed visual quality deterioration by reducing oxidative reactions during storage.

Table 3. Changes in color parameters of uncoated and coated blueberries.

Parameters	Storage days	Control	SA/0.2 HA	SA/0.5 HA	SA/0.2 HA-PE	SA/0.5 HA-PE
L*	0	27.77 ± 1.83^{a}	24.07 ± 1.50^{bc}	26.53 ± 2.24^{ab}	22.50 ± 1.03^{c}	24.43 ± 2.11^{bc}
	2	26.65 ± 1.55^{a}	24.47 ± 2.00^{ab}	27.32 ± 2.09^{a}	21.93 ± 1.53^{b}	24.55 ± 0.58^{ab}
	4	29.97 ± 0.85^{ab}	28.57 ± 2.01^{bc}	31.15 ± 1.39^{a}	27.35 ± 1.13^{c}	28.85 ± 1.00^{abc}
	6	30.43 ± 0.63^{a}	29.68 ± 1.51^{a}	30.88 ± 1.76^{a}	27.43 ± 0.93^{b}	28.97 ± 0.98^{ab}
	8	25.72 ± 1.45^{ab}	24.97 ± 1.97^{ab}	27.55 ± 2.01^{a}	23.12 ± 2.8^{b}	24.28 ± 0.98^{ab}
	10	25.70 ± 0.83^{a}	24.40 ± 1.52^{a}	27.23 ± 2.55^{a}	23.75 ± 3.41^{a}	24.10 ± 1.21^{a}
*a**	0	-0.32 ± 0.16^{ab}	-0.30 ± 0.22^{ab}	-0.40 ± 0.00^{b}	0.00 ± 0.33^{a}	-0.08 ± 0.15^{ab}
	2	-0.43 ± 0.10^{c}	-0.43 ± 0.10^{c}	-0.40 ± 0.09^{bc}	-0.17 ± 0.08^{a}	-0.25 ± 0.05^{ab}
	4	-0.52 ± 0.08^{c}	-0.4 ± 0.10^{bc}	-0.48 ± 0.10^{c}	-0.10 ± 0.10^{a}	-0.28 ± 0.03^{b}
	6	-0.38 ± 0.10^{b}	-0.37 ± 0.14^{b}	-0.42 ± 0.19^{b}	0.08 ± 0.32^{a}	-0.15 ± 0.10^{ab}
	8	-0.42 ± 0.14^{b}	-0.43 ± 0.03^{b}	-0.50 ± 0.05^{b}	0.60 ± 1.22^{a}	-0.23 ± 0.10^{ab}
	10	-0.17 ± 0.26^{ab}	-0.22 ± 0.24^{b}	-0.20 ± 0.23^{b}	0.27 ± 0.28^{a}	0.03 ± 0.28^{ab}
b*	0	-5.42 ± 0.93^{b}	-4.40 ± 1.38^{ab}	-4.22 ± 0.36^{ab}	-3.53 ± 0.68^{a}	-3.65 ± 0.39^{a}
	2	-5.20 ± 1.02^{c}	-3.67 ± 0.90^{abc}	-4.83 ± 1.58^{bc}	-2.98 ± 0.51^{a}	-3.35 ± 0.26^{ab}
	4	-4.63 ± 0.21^{b}	-3.32 ± 0.73^{a}	-3.53 ± 0.25^{a}	-2.93 ± 0.42^{a}	-3.08 ± 0.20^{a}
	6	-4.60 ± 0.31^{b}	-3.13 ± 0.96^{a}	-3.68 ± 0.33^{ab}	-2.85 ± 0.45^{a}	-3.03 ± 0.39^{a}
	8	-4.77 ± 0.50^{b}	-3.35 ± 0.88^{a}	-3.78 ± 0.20^{ab}	-2.97 ± 0.94^{a}	-2.97 ± 0.33^{a}
	10	-4.72 ± 0.45^{b}	-3.35 ± 0.85^{a}	-3.62 ± 0.20^{ab}	-2.80 ± 0.58^{a}	-2.98 ± 0.98^{a}

Means with different letters (a, b, c) on the same row indicate significant differences ($p < 0.05$) according to Fisher's LSD test.

3.2.3. Changes in pH and total soluble solids (TSS)

The pH of blueberries varied during storage, with coated fruits generally maintaining more stable values than the control. The control exhibited greater fluctuations, ranging from 3.38 to 3.79, whereas the coated samples showed between 3.53 and 3.92 (Table 4). Notably, the SA/0.5 HA treatment reached the highest pH (3.92) on day 8, while SA/0.5 HA-PE maintained relatively stable values (3.57–3.74) throughout storage. These changes may reflect differences in the metabolic progression of the coated fruit during storage. Edible coatings can act as semi-permeable barriers that modify the transfer of water vapor and respiratory gases, and such regulation may potentially influence postharvest metabolic processes (Lee et al., 2024). In the present study, however, oxygen consumption, carbon dioxide production, and gas permeability of the coatings were not directly measured. Therefore, the relatively stable pH values should be interpreted as being consistent with delayed physicochemical deterioration, while any specific reduction in respiration or alteration of gas exchange remains to be experimentally confirmed. Similar findings were reported by (Shi et al., 2025), who observed that curcumin/β-cyclodextrin Pickering emulsion coatings helped maintain blueberry pH during storage.

Total soluble solids (TSS), an indicator of sweetness and fruit maturity, increased significantly in all treatments during storage, reflecting normal ripening progression. The control increased from 1.20% to 1.57%, while coated fruits reached final values between 1.50% and 1.70% (Table 4). The highest TSS was observed in the SA/0.2 HA-PE treatment (1.70%) on days 8 and 10, whereas SA/0.5 HA-PE maintained a lower value of 1.50% at the end of storage. The observed changes in pH and TSS indicate differences in the

physicochemical progression of the coated blueberries during storage and may be associated with differences in postharvest quality retention. The increase in TSS is attributed to sugar breakdown during ripening (Li et al., 2025; Piechowiak et al., 2022).

Table 4. pH and total soluble solids (TSS) of uncoated and coated blueberries.

Parameters	Storage days	Control	SA/0.2 HA	SA/0.5 HA	SA/0.2 HA-PE	SA/0.5 HA-PE
pH	0	3.56 ± 0.11^{a}	3.31 ± 0.15^{a}	3.41 ± 0.24^{a}	3.35 ± 0.35^{a}	3.30 ± 0.24^{a}
	2	3.57 ± 0.01^{c}	3.54 ± 0.04^{c}	3.70 ± 0.09^{b}	3.83 ± 0.03^{a}	3.60 ± 0.03^{c}
	4	3.52 ± 0.02^{b}	3.53 ± 0.01^{b}	3.60 ± 0.03^{a}	3.60 ± 0.02^{a}	3.57 ± 0.01^{a}
	6	3.38 ± 0.03^{d}	3.55 ± 0.02^{c}	3.72 ± 0.02^{a}	3.60 ± 0.01^{bc}	3.60 ± 0.04^{b}
	8	3.79 ± 0.02^{bc}	3.71 ± 0.06^{d}	3.92 ± 0.06^{a}	3.84 ± 0.02^{b}	3.74 ± 0.04^{cd}
	10	3.72 ± 0.04^{b}	3.61 ± 0.04^{c}	3.53 ± 0.03^{d}	3.88 ± 0.02^{a}	3.63 ± 0.03^{c}
TSS (%)	0	1.20 ± 0.00^{a}	0.90 ± 0.00^{c}	0.97 ± 0.06^{b}	1.00 ± 0.00^{b}	1.00 ± 0.00^{b}
	2	1.07 ± 0.06^{b}	1.10 ± 0.00^{b}	1.20 ± 0.00^{a}	1.17 ± 0.06^{a}	1.20 ± 0.00^{a}
	4	1.30 ± 0.00^{b}	1.23 ± 0.06^{c}	1.20 ± 0.00^{c}	1.40 ± 0.00^{a}	1.23 ± 0.06^{c}
	6	1.37 ± 0.06^{a}	1.20 ± 0.06^{b}	0.93 ± 0.06^{c}	1.40 ± 0.00^{a}	1.20 ± 0.00^{b}
	8	1.23 ± 0.06^{d}	1.50 ± 0.00^{b}	1.40 ± 0.00^{c}	1.70 ± 0.00^{a}	1.10 ± 0.00^{e}
	10	1.57 ± 0.06^{b}	1.50 ± 0.00^{c}	1.67 ± 0.06^{a}	1.70 ± 0.00^{a}	1.50 ± 0.00^{c}

Means with different letters (a, b, c) on the same row indicate significant differences ($p < 0.05$) according to Fisher's LSD test.

3.3. Correlation structure among blueberry quality attributes during storage

The correlation patterns among blueberry quality attributes provide a clear picture of how fruits responded to storage and how the SA/HA coatings with or without Pickering-emulsion reinforcement modulated these responses (Fig. 10). The strong negative correlation between weight loss and firmness ($r = –0.742$) indicates that treatments associated with lower mass loss also tended to retain greater firmness during storage. Biologically, this association is consistent with the possibility that reduced dehydration help reduced helped maintain cellular water status and delayed structural deterioration. However, correlation does not establish causality, and firmness is also affected by cell-wall degradation and other physiological processes. Therefore, the correlation should be interpreted as evidence of an association between moisture loss and firmness retention rather than proof that reduced weight loss directly caused the preservation of firmness. The positive correlation between TSS and pH ($r = 0.706$) indicates that these two quality attributes tended to increase together during storage. This association may reflect coordinated changes in fruit ripening and physicochemical status; however, it should be interpreted cautiously because titratable acidity (TA), which provides a measure of the total acid content, was not determined. Therefore, the observed correlation between TSS and pH should be regarded as an association among the measured quality attributes rather than evidence of a direct relationship between sugar accumulation and acidity changes. Moderate positive correlations between TSS and color parameters suggest that pigment changes and sugar metabolism progressed together. Coatings that slowed moisture loss and respiration therefore helped stabilize both internal biochemical composition and external appearance. Color attributes showed additional associations with

firmness and TSS. Berries that softened more rapidly tended to darken and shift toward red hues, reflecting anthocyanin accumulation during senescence. By slowing softening, the coatings indirectly supported color stability through reduced cuticle stress and moderated pigment oxidation. Moderate correlations between L* and both TSS and pH further indicate that berries with slower metabolic progression retained a lighter, fresher appearance—an important factor for consumer acceptance.

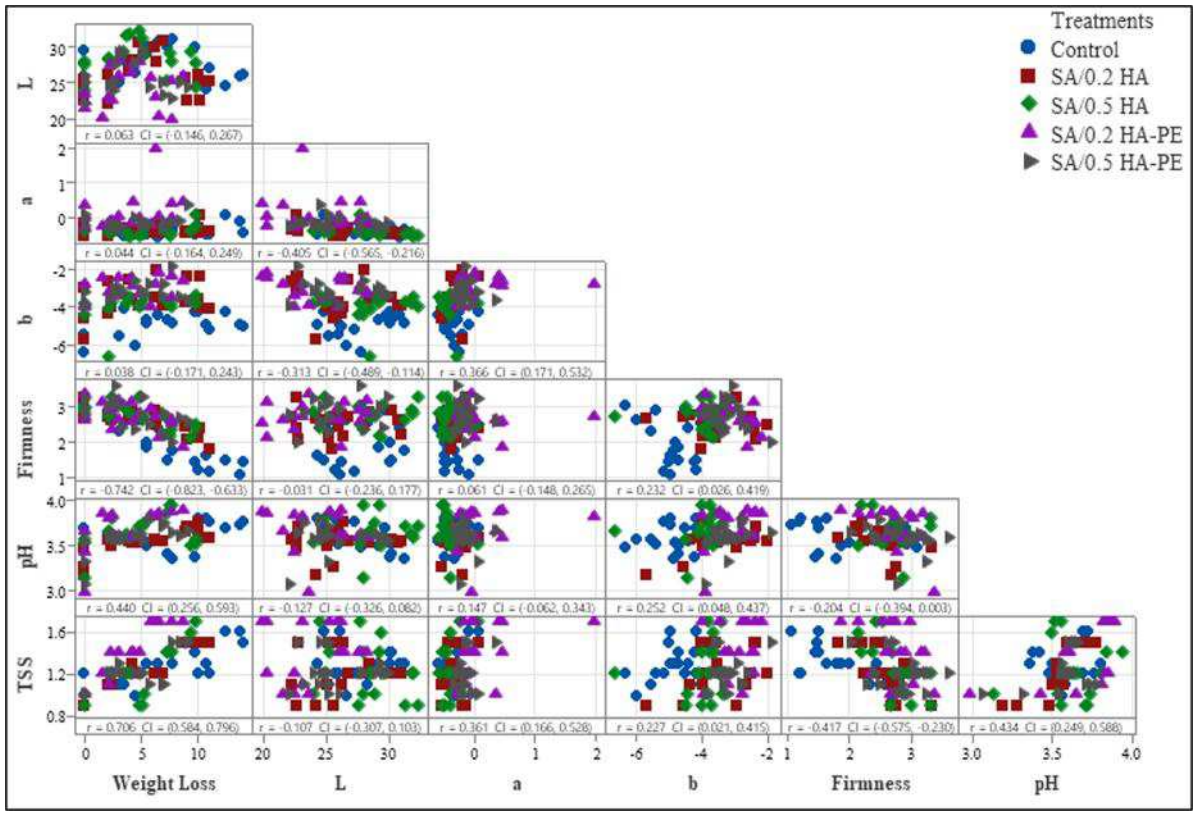


Fig. 10. Correlogram showing Pearson correlations among blueberry quality attributes during storage.

3.4. Principal Component Analysis of blueberry quality attributes

The loading plot showed that weight loss, TSS, and pH were positively associated with PC1, whereas firmness was negatively correlated (Fig. 11A), demonstrating that increased

ripening and water loss were accompanied by a reduction in fruit firmness. The L* value was mainly associated with PC2, while the *a** and b* color coordinates clustered together, indicating a close relationship between color changes during storage. The PCA provided an integrated view of the relationships among the measured postharvest quality attributes. PC1 accounted for 37.2% of the total variance and was associated primarily with variables related to physical deterioration, particularly weight loss and firmness. This axis can therefore be interpreted as representing a general dimension of structural and moisture-related quality changes during storage. PC2 explained an additional 26.4% of the variance and was more strongly associated with physicochemical attributes such as TSS and pH, reflecting differences in the biochemical progression of fruit quality during storage. The separation of coated and uncoated samples along these components suggests that the coating treatments were associated with different trajectories of physical and physicochemical deterioration (Fig. 11B). Importantly, PCA is an exploratory multivariate tool and does not by itself establish causal mechanisms. The biological interpretation should therefore be considered an indication of coordinated quality changes rather than direct evidence of a specific physiological pathway.

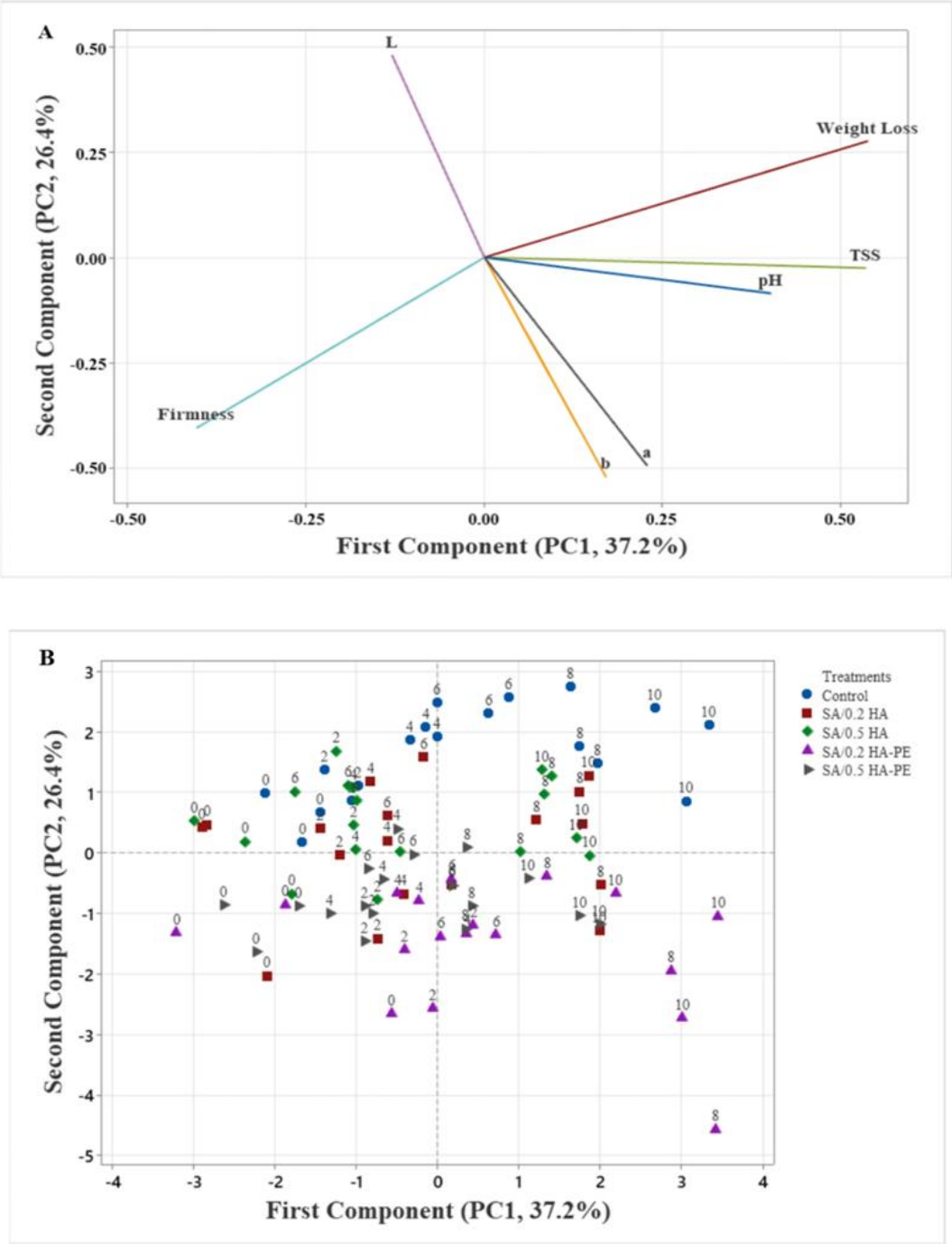


Fig. 11. Principal Component Analysis (PCA) of blueberry quality attributes under different coating treatments. (**A**) PCA loading and (**B**) score plot.

4. Conclusion

This study developed a hyaluronic acid (HA)-functionalized, cellulose nanofiber (CNF)-stabilized Pickering emulsion edible coating based on sodium alginate for blueberry preservation. The developed formulations showed good physical stability, favorable oil-binding capacity, and successful incorporation of the Pickering emulsion into the sodium alginate–HA matrix. Among the formulations evaluated, SA/0.5 HA-PE exhibited a relatively homogeneous microstructure, favorable moisture-barrier properties, enhanced UV-light shielding, and strong antifungal activity against *Botrytis cinerea*. Application of the coatings to blueberries reduced weight loss and helped maintain firmness and visual quality during 10 days of storage at 25 °C. The observed relationships among coating properties and postharvest quality attributes further demonstrate the multifunctional nature of the coating system. Overall, the findings indicate that HA-functionalized CNF Pickering emulsions can be incorporated into sodium alginate films to develop multifunctional edible coatings with potential application in postharvest preservation. However, because formulations without HA and a non-ultrasound control were not included, the independent contributions of HA and ultrasound cannot be established from the present study. Further studies incorporating formulations without HA and a non-ultrasound control should be done.

CRediT authorship contribution statement

R.M.A. Kholiq: Data curation, Formal analysis, Investigation, Methodology, Validation, Visualization, Writing – original draft. **F.N. Nkede:** Conceptualization, Data curation, Formal analysis, Investigation, Methodology, Supervision, Validation, Writing – original draft, Writing – review and editing. **M.H. Wardak:** Investigation. **A. Bibi:** Writing – original

draft. **F. Meng:** Investigation. **A.A. Wardana:** Writing – review and editing. **F. Tanaka:** Supervision, Funding acquisition, Validation and **F. Tanaka:** Supervision, Funding acquisition, Writing – review and editing, Validation.

Declaration of conflict of interest

The authors did not have any conflict of interest to declare.

Funding

This research was funded by the Fuji Seal Foundation.

Data Availability Statement

All data produced or examined in this study are fully presented within this manuscript and its accompanying supplementary files.

References

Abbaszadeh, M., Arsalani, N., Kazeminava, F., & Mahoutforoush, A. (2025). Incorporating halloysite nanotubes@malva extract into Starch-Hyaluronic acid nanocomposite films containing carbon quantum dots for antibacterial application. *Carbohydrate Polymer Technologies and Applications*, *11*. https://doi.org/10.1016/j.carpta.2025.100906

Alemdar, N. (2016). Fabrication of a novel bone ash-reinforced gelatin/alginate/hyaluronic acid composite film for controlled drug delivery. *Carbohydrate Polymers*, *151*, 1019–1026. https://doi.org/10.1016/j.carbpol.2016.06.033

Al-Hilifi, S. A., Al-Ali, R. M., Dinh, L. N. M., Yao, Y., & Agarwal, V. (2024). Development of hyaluronic acid based polysaccharide-protein composite edible coatings for preservation of strawberry fruit. *International Journal of Biological Macromolecules*, *259*. https://doi.org/10.1016/j.ijbiomac.2023.128932

Ali, M., Ali, A., Ali, S., Chen, H., Wu, W., Liu, R., et al. (2025, January 1). Global insights and advances in edible coatings or films toward quality maintenance and reduced postharvest losses of fruit and vegetables: An updated review. *Comprehensive Reviews in Food Science and Food Safety* . John Wiley and Sons Inc. https://doi.org/10.1111/1541-4337.70103

Ashique, S., Mukherjee, T., Mohanty, S., Garg, A., Mishra, N., Kaushik, M., et al. (2024). Blueberries in focus: Exploring the phytochemical potentials and therapeutic applications. *Journal of Agriculture and Food Research*, *18*. https://doi.org/10.1016/j.jafr.2024.101300

Bibi, A., Nkede, F. N., Van, T. T., Wardak, M. H., Fanze, M., Ullah, S., et al. (2026a). Multifunctional fermented cassava starch–chitosan films and coatings loaded with Hyssopus officinalis essential oil: Development, properties, postharvest preservation of cherry tomatoes. *Progress in Organic Coatings*, *217*. https://doi.org/10.1016/j.porgcoat.2026.110224

Bibi, A., Nkede, F. N., Van, T. T., Wardak, M. H., Fanze, M., Ullah, S., et al. (2026b). Multifunctional fermented cassava starch–chitosan films and coatings loaded with Hyssopus officinalis essential oil: Development, properties, postharvest preservation of cherry tomatoes. *Progress in Organic Coatings*, *217*. https://doi.org/10.1016/j.porgcoat.2026.110224

Cao, S., Qiao, L., Wang, X., Huang, T., Wu, C., Zhang, Y., et al. (2025). Discussion on postharvest quality, strategies of storage and transportation techniques of blueberries: A comprehensive review. *Food Quality and Safety*. Oxford University Press. https://doi.org/10.1093/fqsafe/fyaf038

Cao, X., Tang, Y., Dai, J., An, K., Tian, T., Tong, X., et al. (2026). Soybean whey protein-hyaluronic acid low-fat digestibility oleogel: Interactions, network structure, and functional properties. *Food Hydrocolloids*, *179*. https://doi.org/10.1016/j.foodhyd.2026.112775

Cheng, H., Zhang, C., Wang, J., & Xie, J. (2024). Effects of orthogonal dual-frequency ultrasound-assisted treatment combined with bioactive coating containing Melissa officinalis L. essential oil on changes in quality, lipid, and protein of large yellow croaker (Pseudosciaena crocea) during cold storage. *Food Chemistry: X*, *24*. https://doi.org/10.1016/j.fochx.2024.101861

Das, S. K., Vishakha, K., Das, S., Chakraborty, D., & Ganguli, A. (2022). Carboxymethyl cellulose and cardamom oil in a nanoemulsion edible coating inhibit the growth of foodborne pathogens and extend the shelf life of tomatoes. *Biocatalysis and Agricultural Biotechnology*, *42*. https://doi.org/10.1016/j.bcab.2022.102369

Das, S., Vishakha, K., Banerjee, S., Mondal, S., & Ganguli, A. (2020). Sodium alginate-based edible coating containing nanoemulsion of Citrus sinensis essential oil eradicates planktonic and sessile cells of food-borne pathogens and increased quality attributes of tomatoes. *International Journal of Biological Macromolecules*, *162*, 1770–1779. https://doi.org/10.1016/j.ijbiomac.2020.08.086

Ding, J., Liu, C., Huang, P., Li, H., Liu, Y., Sameen, D. E., et al. (2024a). Effects of konjac glucan-nan/low-acyl gellan edible coatings loaded thymol-β-cyclodextrin microcapsules on postharvest blueberry. *Food Chemistry*, *430*. https://doi.org/10.1016/j.foodchem.2023.137080

Ding, J., Liu, C., Huang, P., Li, H., Liu, Y., Sameen, D. E., et al. (2024b). Effects of konjac glucan-nan/low-acyl gellan edible coatings loaded thymol-β-cyclodextrin microcapsules on postharvest blueberry. *Food Chemistry*, *430*. https://doi.org/10.1016/j.foodchem.2023.137080

El-Aassar, M. R., El-Beheri, N. G., Agwa, M. M., Eltaher, H. M., Alseqely, M., Sadik, W. S., & El-Khordagui, L. (2021). Antibiotic-free combinational hyaluronic acid blend nanofibers for wound healing enhancement. *International Journal of Biological Macromolecules*, *167*, 1552–1563. https://doi.org/10.1016/j.ijbiomac.2020.11.109

855 Fei, X., Yang, S., Gong, D., & Zhang, G. (2026). Hydrophobic modification of chitosan-
856 carrageenan film with cinnamon essential oil Pickering emulsion: Improving
857 mechanical properties and fresh-keeping effect on blueberry. *Innovative Food Science*
858 *and Emerging Technologies*, *111*. https://doi.org/10.1016/j.ifset.2026.104578

859 Guo, Y., Yang, X., Bao, Y. hong, Zhao, X. lei, Huang, L., Chen, Z. xiang, et al. (2022).
860 Investigation of the in vitro digestion fate and oxidation of protein-based oleogels
861 prepared by pine nut oil. *LWT*, *164*. https://doi.org/10.1016/j.lwt.2022.113660

862 Ji, R., Guo, H., Yang, X., Wang, L., Zhang, X., & Zhang, H. (2026). Chitosan/gelatin-based
863 film activated by Pickering emulsion of citrus essential oil stabilized by esterified
864 starch/whey protein isolate fibrils: Application in preserving freshness of blueberry.
865 *Food Chemistry*, *503*. https://doi.org/10.1016/j.foodchem.2026.147848

866 Jiang, X., Ding, J., Guo, L., Chu, X., Zhao, Y., Chen, M., et al. (2023). Effects of H.uvarum
867 combined with KGM on postharvest diseases of blueberry. *Food Bioscience*, *53*.
868 https://doi.org/10.1016/j.fbio.2023.102730

869 Kim, S., Cho, D. H., Kweon, D. K., Jang, E. H., Hong, J. Y., & Lim, S. T. (2020).
870 Improvement of mechanical properties of orodispersible hyaluronic acid film by
871 carboxymethyl cellulose addition. *Food Science and Biotechnology*, *29*(9), 1233–1239.
872 https://doi.org/10.1007/s10068-020-00771-1

873 Kobasy, W., Gong, X., Elshamandy, N. K. F., Zahran, H. A., Osman, A. I., & Rashwan, A. K.
874 (2025). ATR-FTIR, DSC, GC–MS of garlic (Allium sativum), parsley (Petroselinum
875 crispum), and thyme (Thymus vulgaris) essential oils and their synergistic effects on
876 antioxidant and antimicrobial properties. *Food Bioscience*, *71*.
877 https://doi.org/10.1016/j.fbio.2025.107262

878 Kusuma, G., Marcellino, V., Wardana, A. A., Wigati, L. P., Liza, C., Wulandari, R., et al.
879 (2024). Biofunctional features of Pickering emulsified film from citrus peel
880 pectin/limonene oil/nanocrystalline cellulose. *International Journal of Food Science*
881 *and Technology*. https://doi.org/10.1111/ijfs.17049

Lee, D., Gwon, J., Huang, R., Picha, D. H., & Wu, Q. (2024). Bio-based nanomaterial suspensions as sprayable coatings for maintaining blueberry postharvest quality. *Food Hydrocolloids*, *150*. https://doi.org/10.1016/j.foodhyd.2024.109743

Li, J., Liu, G., Huang, Y., Pan, Q., Bai, Z., Li, C., et al. (2025). Comprehensive evaluation of optimized preservation strategies for blueberries: An assessment of diverse intervention measures based on network meta-analysis. *Scientia Horticulturae*, *351*. https://doi.org/10.1016/j.scienta.2025.114380

Li, Yang, Rokayya, S., Jia, F., Nie, X., Xu, J., Elhakem, A., et al. (2021). Shelf-life, quality, safety evaluations of blueberry fruits coated with chitosan nano-material films. *Scientific Reports*, *11*(1). https://doi.org/10.1038/s41598-020-80056-z

Li, Yuxuan, Rong, H., Lin, S., Zheng, Y., Yang, L., Sun, B., et al. (2025). Hydrogel pads loaded with essential oil contribute to maintaining blueberry quality after transportation. *Food Packaging and Shelf Life*, *51*. https://doi.org/10.1016/j.fpsl.2025.101587

Liu, M., Zhang, Y., Shi, L., Li, P., Zhang, B., Zhang, X., & Liu, S. (2025). Development of Ultrasound-Assisted Doped with White Round Grapefruit Essential Oil Bilayer Films for Lycium barbarum Preservation. *ACS Omega*, *10*(21), 21350–21360. https://doi.org/10.1021/acsomega.4c11630

Liu, Yang, Ren, L., & Wang, Y. (2013). Crosslinked collagen-gelatin-hyaluronic acid biomimetic film for cornea tissue engineering applications. *Materials Science and Engineering C*, *33*(1), 196–201. https://doi.org/10.1016/j.msec.2012.08.030

Liu, Yu, Wang, J., Ma, N., Guo, G., Kumar, R., Wu, H., & Tian, H. (2026). Development of Bio-Based Edible Films for Meat Preservation: A Study on the Application of Carvacrol Microcapsules Combined With Hyaluronic Acid and Gelatin. *Journal of Food Processing and Preservation*, *2026*(1). https://doi.org/10.1155/jfpp/3038234

907 Ma, Y., Ye, F., Chen, J., Ming, J., Zhou, C., Zhao, G., & Lei, L. (2023). The microstructure
908 and gel properties of linseed oil and soy protein isolate based-oleogel constructed with
909 highland barley β-glucan and its application in luncheon meat. *Food Hydrocolloids*, *140*.
910 https://doi.org/10.1016/j.foodhyd.2023.108666

911 Mai, X., Yang, Y., Wang, D., Xu, W., Sun, Z., & Liu, F. (2025). Novel dual-crosslinked
912 antimicrobial hydrogels of oxidized hyaluronic acid/gelatin grafted with curcumin-
913 Zn2+ complexes for preservation of chilled chicken. *Food Packaging and Shelf Life*, *49*.
914 https://doi.org/10.1016/j.fpsl.2025.101519

915 Meng, F., Yan, X., Nkede, F. N., Wardak, M. H., Van, T. T., Tanaka, F., & Tanaka, F. (2024).
916 An intelligent chitosan/polyvinyl alcohol film with two types of anthocyanins for
917 improved color recognition accuracy and monitoring fresh-cut pineapple freshness.
918 *Food Packaging and Shelf Life*, *46*. https://doi.org/10.1016/j.fpsl.2024.101402

919 Meng, F., Yan, X., Van, T. T., Nkede, F. N., Wardak, M. H., Tanaka, F., & Tanaka, F. (2026).
920 Development of a UV-cured intelligent film based on sodium alginate/polyvinyl alcohol,
921 Nano-TiO_2, and anthocyanins extracted from purple Asparagus for Salmon freshness
922 assessment. *Innovative Food Science and Emerging Technologies*, *107*.
923 https://doi.org/10.1016/j.ifset.2025.104366

924 Meng, F., Yan, X., Zeng, J., Tanaka, F., & Tanaka, F. (2025). Development of sodium
925 alginate-titanium dioxide films incorporating anthocyanin for antibacterial and
926 freshness sensing applications. *LWT*, *229*. https://doi.org/10.1016/j.lwt.2025.118198

927 Mohamed, A. M. A., & Ramaswamy, H. S. (2025). Caseinate–Carboxymethyl Chitosan
928 Composite Edible Coating with Soybean Oil for Extending the Shelf Life of Blueberry
929 Fruit. *Foods*, *14*(15). https://doi.org/10.3390/foods14152598

930 Montes-Ramírez, P., Montaño-Leyva, B., Blancas-Benitez, F. J., Bautista-Rosales, P. U.,
931 Ruelas-Hernández, N. D., Martínez-Robinson, K., & González-Estrada, R. R. (2024).
932 Active films and coatings based on commercial chitosan with natural extracts addition

from coconut by-products: Physicochemical characterization and antifungal protection on tomato fruits. *Food Control*, *155*. https://doi.org/10.1016/j.foodcont.2023.110077

Nkede, F. N., Wardak, M. H., Fanze, M., Kondo, N., Wardana, A. A., Jothi, J. S., et al. (2024a). The potential of helichrysum italicum essential oil-infused alginate coatings and film for prolonging the shelf-life of cherry tomatoes. *Food Packaging and Shelf Life*, *46*. https://doi.org/10.1016/j.fpsl.2024.101381

Nkede, F. N., Wardak, M. H., Wardana, A. A., Fanze, M., Yan, X., Jothi, J. S., et al. (2024a). Preparation and characterization of edible coating and film composed of sodium alginate/ylang-ylang oil/cellulose nanocrystals Pickering emulsion and its application to post-harvest control of mandarin (Citrus reticulata). *Colloids and Surfaces A: Physicochemical and Engineering Aspects*, *691*. https://doi.org/10.1016/j.colsurfa.2024.133859

Nkede, F. N., Wardana, A. A., Phuong, N. T. H., Takahashi, M., Koga, A., Wardak, M. H., et al. (2023a). Preparation and Characterization of Chitosan/Lemongrass Oil/Cellulose Nanofiber Pickering Emulsions Active Packaging and Its Application on Tomato Preservation. *Journal of Polymers and the Environment*, *31*(11), 4930–4945. https://doi.org/10.1007/s10924-023-02885-z

Nkede, F. N., Wardana, A. A., Phuong, N. T. H., Xirui, Y., Koga, A., Wardak, M. H., et al. (2023b). Improved alginate-based films by Ylang-ylang (Cananga odorata L) oil incorporation. *Polymers for Advanced Technologies*, *34*(7), 2213–2223. https://doi.org/10.1002/pat.6042

Panahi, Z., & Mohsenzadeh, M. (2022). Sodium alginate edible coating containing Ferulago angulata (Schlecht.) Boiss essential oil, nisin, and NaCl: Its impact on microbial, chemical, and sensorial properties of refrigerated chicken breast. *International Journal of Food Microbiology*, *380*. https://doi.org/10.1016/j.ijfoodmicro.2022.109883

Phuong, N. T. H., Koga, A., Nkede, F. N., Tanaka, F., & Tanaka, F. (2023). Application of edible coatings composed of chitosan and tea seed oil for quality improvement of

960 strawberries and visualization of internal structure changes using X-ray computed
961 tomography. *Progress in Organic Coatings*, *183*.
962 https://doi.org/10.1016/j.porgcoat.2023.107730

963 Piechowiak, T., Grzelak-Błaszczyk, K., Sójka, M., Skóra, B., & Balawejder, M. (2022).
964 Quality and antioxidant activity of highbush blueberry fruit coated with starch-based
965 and gelatine-based film enriched with cinnamon oil. *Food Control*, *138*.
966 https://doi.org/10.1016/j.foodcont.2022.109015

967 Porat, R., Lichter, A., Terry, L. A., Harker, R., & Buzby, J. (2018, May 1). Postharvest losses
968 of fruit and vegetables during retail and in consumers' homes: Quantifications, causes,
969 and means of prevention. *Postharvest Biology and Technology*. Elsevier B.V.
970 https://doi.org/10.1016/j.postharvbio.2017.11.019

971 Santos, S. F. dos, Cardoso, R. de C. V., Borges, Í. M. P., Almeida, A. C. e., Andrade, E. S.,
972 Ferreira, I. O., & Ramos, L. do C. (2020). Post-harvest losses of fruits and vegetables
973 in supply centers in Salvador, Brazil: Analysis of determinants, volumes and reduction
974 strategies. *Waste Management*, *101*, 161–170.
975 https://doi.org/10.1016/j.wasman.2019.10.007

976 Semeniuc, C. A., Pop, C. R., & Rotar, A. M. (2017). Antibacterial activity and interactions
977 of plant essential oil combinations against Gram-positive and Gram-negative bacteria.
978 *Journal of Food and Drug Analysis*, *25*(2), 403–408.
979 https://doi.org/10.1016/j.jfda.2016.06.002

980 Sgorla, D., Almeida, A., Azevedo, C., Bunhak, É. J., Sarmento, B., & Cavalcanti, O. A.
981 (2016). Development and characterization of crosslinked hyaluronic acid polymeric
982 films for use in coating processes. *International Journal of Pharmaceutics*, *511*(1), 380–
983 389. https://doi.org/10.1016/j.ijpharm.2016.07.033

984 Shen, Y., Ni, Z. J., Thakur, K., Zhang, J. G., Hu, F., & Wei, Z. J. (2021). Preparation and
985 characterization of clove essential oil loaded nanoemulsion and pickering emulsion

activated pullulan-gelatin based edible film. *International Journal of Biological Macromolecules*, *181*, 528–539. https://doi.org/10.1016/j.ijbiomac.2021.03.133

Shi, S., Tang, J., Zhou, Y., Huang, H., Zhang, J., Liu, W., et al. (2025). Development of sodium alginate-based active packaging films reinforced with curcumin/β-cyclodextrin stabilized high internal phase Pickering emulsions for blueberry preservation. *International Journal of Biological Macromolecules*, *321*. https://doi.org/10.1016/j.ijbiomac.2025.146365

Staropoli, A., Vassetti, A., Salvatore, M. M., Andolfi, A., Prigigallo, M. I., Bubici, G., et al. (2021). Improvement of nutraceutical value of parsley leaves (Petroselinum crispum) upon field applications of beneficial microorganisms. *Horticulturae*, *7*(9). https://doi.org/10.3390/horticulturae7090281

Stull, A. J., Cassidy, A., Djousse, L., Johnson, S. A., Krikorian, R., Lampe, J. W., et al. (2024). The state of the science on the health benefits of blueberries: a perspective. *Frontiers in Nutrition*, *11*. https://doi.org/10.3389/fnut.2024.1415737

Takahashi, M., Nkede, F. N., Tanaka, F., & Tanaka, F. (2024). Development and characterization of mung bean starch and citric acid active packaging combined with terpinen-4-ol and its application to strawberry preservation. *Journal of Food Measurement and Characterization*. https://doi.org/10.1007/s11694-024-02355-7

Wang, J. D., Yang, S. L., Liu, G. S., Zhou, Q., Fu, L. N., Gu, Q., et al. (2024). A degradable multi-functional packaging based on chitosan/silk fibroin via incorporating cellulose nanocrystals-stabilized cinnamon essential oil pickering emulsion. *Food Hydrocolloids*, *153*. https://doi.org/10.1016/j.foodhyd.2024.109978

Wang, L., Xue, H., Ling, Y., Zhong, X., Li, K., Zheng, Q., et al. (2026). Chitosan-Based Composite Films Reinforced with Zein–Inulin–Thyme Essential Oil Pickering Emulsion for Enhanced Structural Integrity and Preservation Capacity. *Foods*, *15*(3). https://doi.org/10.3390/foods15030484

Wang, M., Miao, X., Guo, F., Deng, Z., Bian, F., Xiao, T., & Chen, C. (2024). Optimized hybrid edible surface coating prepared with gelatin and cellulose nanofiber for cherry tomato preservation. *International Journal of Biological Macromolecules*, *279*. https://doi.org/10.1016/j.ijbiomac.2024.134822

Wang, N., Zhao, X., Jiang, Y., Ban, Q., & Wang, X. (2023). Enhancing the stability of oil-in-water emulsions by non-covalent interaction between whey protein isolate and hyaluronic acid. *International Journal of Biological Macromolecules*, *225*, 1085–1095. https://doi.org/10.1016/j.ijbiomac.2022.11.170

Wang, Y., Ma, Z., Liu, Y., & Gong, Y. (2026). Ultrasound-modified soy protein-hyaluronic acid conjugates for swallowing-friendly high internal phase pickering emulsion gels: structure, properties, and applications. *Ultrasonics Sonochemistry*, *128*. https://doi.org/10.1016/j.ultsonch.2026.107802

Wardak, M. H., Nkede, F. N., Reshaka Kavindi, M. A., Van, T. T., Meng, F., Tanaka, F., & Tanaka, F. (2025). Drying temperature effects on oil dispersion and properties of alginate-kiwi seed oil films. *Journal of Food Engineering*, *400*. https://doi.org/10.1016/j.jfoodeng.2025.112644

Wardak, M. H., Nkede, F. N., Van, T. T., Meng, F., Xirui, Y., Jothi, J. S., et al. (2024). Development of a coating material composed of sodium alginate and kiwifruit seed essential oil to enhance persimmon fruit quality using a novel partial coating technique. *Food Packaging and Shelf Life*, *45*. https://doi.org/10.1016/j.fpsl.2024.101331

Wardana, A. A., Koga, A., Tanaka, F., & Tanaka, F. (2021). Antifungal features and properties of chitosan/sandalwood oil Pickering emulsion coating stabilized by appropriate cellulose nanofiber dosage for fresh fruit application. *Scientific Reports*, *11*(1). https://doi.org/10.1038/s41598-021-98074-w

Wardana, A. A., Wigati, L. P., Marcellino, V., Kusuma, G., Yan, X. R., Nkede, F. N., et al. (2024). The incorporation of chitosan nanoparticles enhances the barrier properties and antifungal activity of chitosan-based nanocomposite coating films. *International*

1039 *Journal of Biological Macromolecules*, *280*.
1040 https://doi.org/10.1016/j.ijbiomac.2024.135840

1041 Wen, J., Zhang, W., Xu, Y., Yu, Y., Lin, X., Fu, M., et al. (2023). Cellulose nanofiber from
1042 pomelo spongy tissue as a novel particle stabilizer for Pickering emulsion. *International*
1043 *Journal of Biological Macromolecules*, *224*, 1439–1449.
1044 https://doi.org/10.1016/j.ijbiomac.2022.10.230

1045 Wigati, L. P., Wardana, A. A., Tanaka, F., & Tanaka, F. (2023). Application of pregelatinized
1046 corn starch and basil essential oil edible coating with cellulose nanofiber as Pickering
1047 emulsion agent to prevent quality-quantity loss of mandarin orange. *Food Packaging*
1048 *and Shelf Life*, *35*. https://doi.org/10.1016/j.fpsl.2022.101010

1049 Wong, P. Y. Y., & Kitts, D. D. (2006). Studies on the dual antioxidant and antibacterial
1050 properties of parsley (Petroselinum crispum) and cilantro (Coriandrum sativum)
1051 extracts. *Food Chemistry*, *97*(3), 505–515.
1052 https://doi.org/10.1016/j.foodchem.2005.05.031

1053 Wu, J., Gao, Y., Shen, H., Yan, S., Zhao, R., Wang, F., et al. (2024). Application potential of
1054 wheat bran cellulose nanofibers as Pickering emulsion stabilizers and stabilization
1055 mechanisms. *Food Chemistry: X*, *24*. https://doi.org/10.1016/j.fochx.2024.101922

1056 Xu, T., Gao, C. C., Feng, X., Yang, Y., Shen, X., & Tang, X. (2019). Structure, physical and
1057 antioxidant properties of chitosan-gum arabic edible films incorporated with cinnamon
1058 essential oil. *International Journal of Biological Macromolecules*, *134*, 230–236.
1059 https://doi.org/10.1016/j.ijbiomac.2019.04.189

1060 Xu, Y., Chu, Y., Feng, X., Gao, C., Wu, D., Cheng, W., et al. (2020). Effects of zein stabilized
1061 clove essential oil Pickering emulsion on the structure and properties of chitosan-based
1062 edible films. *International Journal of Biological Macromolecules*, *156*, 111–119.
1063 https://doi.org/10.1016/j.ijbiomac.2020.04.027

Zhang, J., Hu, Y., Cai, C., & Tan, Z. (2026). Kenaf cellulose nanofiber-stabilized water-in-water Pickering emulsions enabling bio-based active packaging films: A case of banana and mango preservation. *International Journal of Biological Macromolecules*, *351*. https://doi.org/10.1016/j.ijbiomac.2026.151102

Zhang, Y., Pu, Y., Jiang, H., Chen, L., Shen, C., Zhang, W., et al. (2024). Improved sustained-release properties of ginger essential oil in a Pickering emulsion system incorporated in sodium alginate film and delayed postharvest senescence of mango fruits. *Food Chemistry*, *435*. https://doi.org/10.1016/j.foodchem.2023.137534

Zhou, C., Li, L., Li, D., Zhang, R., Hu, S., Zhong, K., & Yan, B. (2024). Hyaluronic acid-based multifunctional bio-active coating integrated with cinnamaldehyde/hydroxypropyl-β-cyclodextrin inclusion complex for fruit preservation. *International Journal of Biological Macromolecules*, *271*. https://doi.org/10.1016/j.ijbiomac.2024.132605

Živković, J., Petrović, J., El Fadili, M., Pljevljakušić, D., Lebrazi, S., Stojković, D., et al. (2026). Optimizing Antibacterial Essential Oil Blends from Helichrysum plicatum, Petroselinum crispum, and Origanum vulgare for Dairy Preservation: Mixture Design and In Silico Analysis. *Foods*, *15*(4). https://doi.org/10.3390/foods15040675

Supplementary Files

This is a list of supplementary files associated with this preprint. Click to download.

- SupplementaryData1FilmCharacterization.xlsx
- SupplementaryData2PostharvestStorageExperiment.xlsx
- Fig.S1.Contactangleofthefilmsamples.docx